Peer-Reviewed Technical Communication

Propagation and Scattering Effects in Underwater Acoustic Communication Channels

Paul A. van Walree, *Member, IEEE*

***Abstract*—Systematic measurements were performed to characterize shallow-water acoustic propagation channels for applications in the field of underwater communications. The survey was conducted in northern Europe and covers the continental shelf, Norwegian fjords, a sheltered bay, a channel, and the Baltic Sea. The measurements were performed in various frequency bands between 2 and 32 kHz. The outcome of the study is a variety of channels that differ in many ways, defying any attempt to define a typical acoustic communication channel. Miscellaneous forward propagation effects are presented, which are relevant to channel models for the design of modulation schemes, network protocols, and simulation environments.**

***Index Terms*—Acoustic communication, channel sounding, propagation, scattering, signal fluctuations, wideband systems.**

I. Introduction

THE underwater acoustic communication channel is one of the most challenging wireless communication media known to man. There exists no typical acoustic channel, and standard test channels are lacking up to the present day [1]–[3]. The profitable frequency band is limited by ambient noise in the oceans, at predominantly low frequencies [4]–[6], and transmission loss, which increases with frequency and range. A prominent contributor to the frequency dependence of the transmission loss is absorption by seawater, for which there exist various empirical formulas [7]–[10]. Horizontal underwater channels are prone to multipath propagation due to refraction, reflection, and scattering. The sound speed of $c \approx 1.5$ km/s is low compared with the speed of light and may lead to channel delay spreads of tens or hundreds of milliseconds. In some environments, reverberation can persist for seconds. The low speed of sound is also at the origin of significant Doppler effects, which can be subdivided in time-varying frequency shifts and instantaneous frequency spreading. A channel that disperses the signal power in both time and frequency is known as a doubly spread channel [11].

The variation in arrival structures and coherence times is large [12]–[17]. Measurements of probability density functions, for narrowband signal envelopes or for one or more paths in channel impulse response estimates, have revealed Rayleigh [18]–[20], Rician [18], [21], [22], Nakagami-m [22], and K-distributed [23], [24] fading. Studies on the validity of the wide-sense stationary uncorrelated scattering (WSSUS) assumption are relatively rare. There are a few sources that mention [25], [26] or show [15], [27] correlated scattering, and an energy stationarity time of at least 3 min was reported for experiments at the Martha's Vineyard Coastal Observatory (Edgartown, MA, USA) [28]. A *trend*-stationary model was successfully applied to the data examined in [29].

Signal fluctuations occur on various time scales. The responsible mechanisms include seasonal changes in temperature profiles and fish population, fish shoaling, storms, tidal changes in water depth, tidal changes in shear flow or water structure, internal waves, and surface waves [30], [31]. The characteristic time scales of these fluctuations are the seasonal, diurnal, and tidal cycles, minutes in the case of internal waves, and $\approx$10 s for ocean swell. Note that the quantities studied in [30] and [31] are the amplitude and phase of narrowband signals. The channel impulse response is not resolved. A constant signal level can go hand in hand with a fluctuating impulse response. The cycles may be associated with seasonal, diurnal [18], or tidal [32], [33] performance variations of communication systems, but not directly with Doppler spreading or channel tracking by a communications receiver.

Multipath propagation and Doppler effects are recognized as challenges for underwater networking [34], [35], but realistic and computationally attractive models of the physical layer are difficult to realize. The approximation of the acoustic channel in today's network simulations varies from: signal-to-noise ratio (SNR)-based channel models using empirical equations for transmission loss and noise [36]; empirical transmission loss plus the assumption of Rayleigh signal fading [37]; use of ray tracing to more accurately compute the transmission loss for a given scenario [38]; and use of ray tracing to compute a multipath profile and allow for bit errors due to signal self-interference [39]. More involved channel models and simulation tools, which also allow for Doppler effects, have mostly been developed separately from network studies [19], [26], [29], [40]–[46].

The possible causes of Doppler effects, or equivalently a time-varying impulse response, are platform motion and changeability of the propagation medium. The latter category can be subdivided in ocean volume fluctuations and sea-surface dynamics.

Manuscript received November 11, 2012; revised June 10, 2013; accepted August 12, 2013. Date of publication September 20, 2013; date of current version October 09, 2013.

Associate Editor: J. Potter; Guest Editor: J. Preisig.

The author is with the Norwegian Defence Research Establishment (FFI), Horten NO-3191, Norway (e-mail: paul.vanwalree@ffi.no).

Color versions of one or more of the figures in this paper are available online at http://ieeexplore.ieee.org.

Digital Object Identifier 10.1109/JOE.2013.2278913

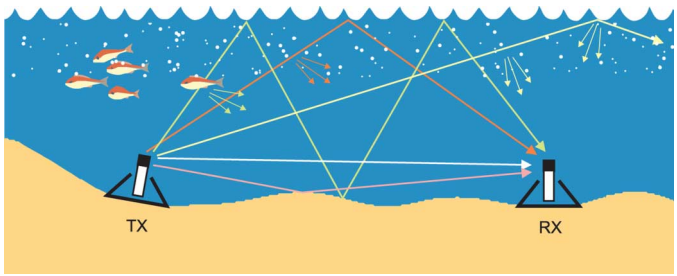

Fig. 1. Depiction of a shallow-water channel with multipath propagation, and scattering by surface waves, air bubbles, and fish.

Platform motion is a straightforward cause of Doppler. Owing to the low sound speed, even small unintended transceiver movements are noticeable at acoustic modem frequencies. The wavelength is of the order of centimeters/decimeters, and the displacement only needs to be a fraction of that to be noticed in the signal phase. The resulting Doppler distortion is much larger than typically seen in wireless radio links and cannot be modeled as a simple frequency shift. Other measures are required for wideband signals [47], [48].

Significant Doppler effects also occur when a modem signal interacts with a dynamic sea surface (Fig. 1). Surface gravity waves have a strong effect on signal propagation [12], [42], [45], [49]–[52], including time-varying path lengths [15], [41], [44], [53]–[55] and corresponding frequency shifts [51], [56], [57]. Even hydrodynamically calm surfaces are important scatterers of acoustic energy at high frequencies [45]. Moreover, diffuse screens and patchy clouds of air bubbles may form under the surface in the presence of breaking waves [58]–[62]. Bubbles scatter and absorb sound, and also modify the sound-speed profile in the top few meters of the water column, thereby enhancing scattering by waves [63]. As the wind speed increases, the bubbles may start to screen the sea surface and reduce the contribution of surface scatter to the received signal energy, yielding a potentially more benign communication channel [62]. On the other hand, in the very shallow waters of the surf zone, dense bubble clouds injected by breaking waves may completely block the channel [2], [61]. The combined effect of wind, waves, and bubbles is a complex matter and can be strongly frequency dependent. Coherence times below 100 ms (at 14 kHz) have occasionally been reported for channels with significant surface interactions [2], [15].

In the absence of platform motion, the variability of refracted paths is governed by volume fluctuations. Sound-speed fluctuations and scattering occur due to internal waves, fish migration, turbulent ship wakes, eddies, river outflows, and other phenomena. Most of the literature studying the effect of volume changes on sound propagation is at low frequencies (below 1 kHz) and long ranges, and reveals coherence times of the order of minutes or longer. Measurements using midfrequency and high-frequency sound are scarce. A coherence time of tens of seconds, at 18 kHz, has been reported due to tidally driven temperature fluctuations [64], and a coherence time of 6 s at 1.6 kHz has been reported due to a packet of strong internal waves traversing the acoustic track [65].[1] Deep refracted paths do not fluctuate as a rule and can be very stable on time scales of relevance to communication systems. This is exploited by time-reversal mirrors, which require the impulse response to remain fairly stable over the two-way travel time between two transceivers [66]. Currents affect the acoustic wavelength rather than the frequency and do not yield Doppler shifts, unless they are time varying. Indirectly, however, currents may cause strong Doppler effects by stirring transceivers [67].

Acoustic communication systems are inherently wideband, as the bandwidth occupied by the signal is not small compared to its center frequency. Frequency-dependent fading statistics, including the mean power, then render narrowband channel models inappropriate and call for more elaborate descriptions [20], [68], [69]. A frequency dependence of the mean received signal power may arise, for instance, due to a frequency dependence of bottom loss [70], [71], surface loss [49], [50], [63], absorption by seawater [7]–[10], and scatterers in the water column [72]. Frequency-dependent fluctuation rates occur when the channel has paths with different Doppler shifts [20], for instance, due to sea-surface interactions and platform motion.

In addition to signal propagation comes ambient noise, from many and varied sources [4]–[6]. Noise at typical acoustic modem frequencies is mostly due to sea-surface agitation: breaking waves, spray, bubble formation and collapse, and rainfall [5]. Anthropogenic noise in this band may come from various sources, such as close shipping and military and mapping sonars. Depending on the setting, sources as diverse as marine mammals, snapping shrimp, cracking ice, and platform self-noise may contribute to the noise field at midfrequencies and high frequencies. Noise statistics may vary significantly between all these sources and are not studied in this paper, which focuses on propagation of the modem signal.

The objective of this paper, which operates on the borderline between acoustics and communications, is to collect in one place a large diversity of channels that may be met by acoustic communication systems. It provides clear examples of channel characteristics mentioned in the literature survey of this introduction, but uses only own measurements for the illustrations and the conclusions. In some cases, the relevance to communications is illustrated by examining the performance or behavior of an adaptive equalizer. Most observations are well known and not new, but some effects and demonstrations are new, or at least not well known.

The paper is organized as follows. Section II describes the employed sounding method and computation of channel parameters. Section III provides a concise overview of the sea trial environments and probe signal parameters. Section IV presents the measurements. It looks at the acoustic channel from different angles, highlighting the diversity of propagation effects, scattering types, and order of magnitude of channel parameters. Finally, Section V summarizes the findings and gives conclusions.

II. Channel Sounding

During the past seven years, measurements were conducted in northern Europe to inventory properties of acoustic communication channels [15]. Channel soundings were performed in different frequency bands and in environments as diverse as bays,

[1]When comparing coherence times from the literature, one should note that different authors use different definitions and computation methods, which are not always disclosed.

fjords, channels, the continental shelf, and the Baltic Sea characterized by its late-summer sound channel. The measurements are systematic in that the same types of probing waveforms and processing are used for all soundings. The purpose of the study is to support research on acoustic channel simulation and modeling, modulation schemes, and network simulations. All channels qualify as horizontal, with water depths ranging from 10 m to a few hundred meters, and a signaling range that is (much) larger than the depth. Soundings are available in various frequency bands between 2 and 32 kHz.

A. Computation

The objective of channel sounding is to measure the channel impulse response $h(t,\tau)$ as a function of time t and time delay τ. A correlative sounder is used with sequential transmission of N pulses of length T' and repetition time T, where a pulse is either a pseudonoise (PN) maximum-length sequence or a linear frequency-modulated (LFM) chirp. The chirp sounder is preferred for sparse ($T' < T$) probes, as the well-known cyclic autocorrelation function of an m-sequence requires $T' = T$. Recorded data are processed in a routine fashion by correlation with the transmit pulse and stacking channel snapshots for successive pulses. The result is an estimate $\hat{h}(t,\tau)$ of the true impulse response $h(t,\tau)$. The estimate is only available for instants $t_n = nT$, $n \in [0, 1, \ldots, N-1]$, measured from the start of the received signal, but continuous-time notation is used for convenience.

Measured channels are examined through various quantities, the estimate $\hat{h}(t,\tau)$ itself, and derived functions: the spreading function, Doppler spectrum, power delay profile, channel correlation function, and phase evolution. Sometimes a simple signal spectrogram can also be very informative.

The spreading function, or delay-Doppler spread function [73], is the Fourier transform of the time-varying impulse response

$$\hat{S}(\upsilon,\tau) = \int_0^{NT} \hat{h}(t,\tau)\exp(-2\pi \mathrm{i}\upsilon t)\,\mathrm{d}t \tag{1}$$

and can be integrated to yield the power delay profile

$$\hat{P}(\tau) = \int_{-1/(2T)}^{1/(2T)} |\hat{S}(\upsilon,\tau)|^2 \mathrm{d}\upsilon = \int_0^{NT} |\hat{h}(t,\tau)|^2 \mathrm{d}t \tag{2}$$

and the Doppler spectrum

$$\hat{P}(\upsilon) = \int_0^{T} |\hat{S}(\upsilon,\tau)|^2 \mathrm{d}\tau\ . \tag{3}$$

$|\hat{S}(\upsilon,\tau)|^2$ is a 2-D density function, which, multiplied by the signal power, gives the distribution of the received power in delay-Doppler space. It is also known as the deterministic scattering function. Its expected value is known as the stochastic scattering function, or simply *the* scattering function. The Doppler spectrum and delay profile are 1-D density functions specifying the distribution of signal power over frequency shift and time delay, respectively.

The scattering function completely characterizes the second-order statistics if the channel satisfies WSSUS [73]. The WSSUS framework was developed for narrowband systems and should be used with caution for acoustic channel characterization. Underwater acoustic communication systems are (ultra)wideband, which violates WSSUS if fading statistics are frequency dependent [68], [69]. Taps in a delay line are then correlated, even if amplitude and phase fluctuations of the physical paths are uncorrelated. Nonstationarity can also occur in acoustic channels. The results in Section IV use the spreading function, because it is not *a priori* given that the scattering function is a meaningful quantity for each channel. The spreading function can be seen as one realization of the scattering function, if the channel would be stationary. The objective of this paper is to show propagation effects, not to apply the WSSUS formalism *per se*.

The issue of stationarity also affects measurements of temporal coherence. There are many ways to estimate or approximate correlation functions [12], [13], [15], and different methods are equivalent under certain conditions. They typically include averaging over the finite observation period of the processes. Averaging improves the estimate in stationary channels, but is less meaningful in nonstationary channels. The outcome is then a good estimate of a channel that never existed. Alternatively, one may consider a short averaging interval, which yields a poorer estimate of a channel that may have existed for a short time. This paper shows correlation functions with and without averaging. A comparison of these two functions provides clues as to the stationarity of the channel.

Let $X(t, t+\Delta t)$ denote the zero-lag cross correlation of two channel snapshots at times t and $t+\Delta t$

$$X(t,t+\Delta t) = \frac{1}{T}\int_0^T \hat{h}^*(t,\tau)\hat{h}(t+\Delta t,\tau)\,\mathrm{d}\tau\ . \tag{4}$$

The expectation of X reads

$$\hat{R}(\Delta t) = \mathbb{E}\left[X(t,t+\Delta t)\right] = \frac{1}{T}\int_0^T \mathbb{E}\left[\hat{h}^*(t,\tau)\hat{h}(t+\Delta t,\tau)\right]\mathrm{d}\tau \tag{5}$$

and is recognized as the channel autocorrelation function averaged over delay. In the computation of $\hat{R}(\Delta t)$, the expectation is approximated by an unbiased estimate of the autocorrelation over the probe signal duration NT.

A normalized "instantaneous correlation" may be defined as

$$\hat{I}(t_0,\Delta t) = \frac{X(t_0,t_0+\Delta t)}{\sqrt{X(t_0,t_0)X(t_0+\Delta t,t_0+\Delta t)}} \tag{6}$$

as a measure of the similarity between impulse response snapshots at a reference instant t_0, and at $t_0+\Delta t$. In Section IV, t_0 is picked as half the duration of the received probe signal. That is, $t_0 = \lceil N/2 \rceil T$, and the time difference $\Delta t \in [-t_0, T-t_0, \ldots, (N-1)T - t_0]$, where the reader is reminded that T is the probe signal pulse spacing.

To investigate correlated scattering, the mean value of $\hat{h}$ is subtracted for all taps

$$\tilde{h}(t,\tau_k) = \hat{h}(t,\tau_k) - \frac{1}{NT}\int_0^{NT} \hat{h}(t,\tau_k)\,\mathrm{d}t \tag{7}$$

and $\tilde{h}(t,\tau_k)$ is used to compute the normalized cross covariance

$$\hat{M}(\tau_k,\tau_l)=\frac{\mathcal{X}(\tau_k,\tau_l)}{\sqrt{\mathcal{X}(\tau_k,\tau_k)\mathcal{X}(\tau_l,\tau_l)}} \tag{8}$$

where

$$\mathcal{X}(\tau_k,\tau_l)=\max_{t'}\left\{\left|\int_0^{NT}\tilde{h}^*(t,\tau_k)\tilde{h}(t+t',\tau_l)\,\mathrm{d}t\right|\right\} \tag{9}$$

is the maximum value of the correlation over the time shift t'. The matrix $\hat{M}(\tau_k,\tau_l)$ gives the correlation strength between amplitude and phase fluctuations of taps at delays τ_k and τ_l. Scattering will be called correlated if the matrix has significant off-diagonal values over a sufficiently long measurement period. The computations use the full duration NT of the sounding.

The last quantity derived from the channel estimate is the residual phase $\hat{\theta}(t,\tau_k)$, defined as the unwrapped phase of $\hat{h}(t,\tau_k)$. In Section IV, it is shown for taps at delays τ_k corresponding to local maxima in the delay profile. It is called residual, because it is computed after Doppler compensation. Platform motion and clock-frequency offsets (CFOs) give rise to true and apparent Doppler shifts, respectively, which can cause a strong phase drift. Before any other processing, these Doppler shifts are removed from the recorded data by resampling.

III. Overview of Data

The results in this paper use *in situ* measurements performed in different frequency bands, geographical areas, seasons, deployment geometries, and use different probe signal parameters. It is not feasible to present the full details for each measurement, but Table I provides basic information. It gives the frequency band of the sounder,[2] the type of probing waveform, the number of pulses N, the pulse duration T', the tracking period T, the in-band SNR of the received signal, range and depth, environment, and time of year. It also says whether there is platform motion and how the Doppler compensation is applied.

The depth in the table is a characteristic value, like the mean value of the transmitter and receiver depths, or the mean water depth in between. No platform motion means that the sender and the receiver were rigidly mounted on stationary bottom frames, as in Fig. 1. Platform motion (yes) means either intentional motion (sender towed by a ship) or unintentional motion (movement of a mooring due to currents or sea state). Section IV-L shows that unintentional platform motion can induce large Doppler effects even for a bottom mooring. In the absence of platform motion, measured channel fluctuations can be attributed to variability of the propagation medium itself.

Accurate Doppler compensation is of critical importance for phase measurements. A stationary deployment is a necessary but not sufficient condition to study phase changes due to the medium, because clock and sampling frequencies of scientific instruments can differ from their nominal (assumed) values. A deviation of only 1 part per million (ppm) is enough to produce a noticeable (linear) phase drift with corresponding Doppler shift and artificial cross-tap correlation. In the processing, CFOs are, therefore, removed by resampling the received signal with a calibrated resampling factor. Alternatively, one may use a common sampling clock to drive the transmitter and the data acquisition systems [30], [74]. The advent of chip-scale atomic clocks may eliminate CFO concerns in the future [75].

Platform kinematics, on the other hand, result in true Doppler shifts that are often time varying. In that case, a nominal Doppler shift is removed by resampling, using a resampling factor that shifts either the peak value (PV) or the center of gravity (COG) of the measured Doppler spectrum to 0 Hz. The last column in Table I says which of the three compensation methods is used.

[2]The probe signals in the table have different spectra. The frequency band is specified as the full width of the main lobe.

IV. Diversity of Channels

The results in this section are grouped by propagation effect, observable, cause, or environment, although there is unavoidable overlap. Figures using a decibel scale present dimensionless normalized quantities, i.e., relative to the maximum value. Axis and decibel ranges are adjusted so as to best highlight the effect under examination.

It is important to realize that all shown results are estimates, and that correlative channel sounders are subject to systematic measurement errors [76]. Channel estimation errors are unavoidable, and, therefore, present in the data, but to the knowledge of the author, these do not invalidate the presented effects. Great care has been taken in the processing to ensure correctness of the observations, whereas this is only partly true for the explanations as to their physical causes. Some measurements are snapshots from long-term experiments with cyclic transmissions of various probe and communications signals, and a collection of environmental data. These data and their analyses cannot be included, but justify some of the statements. For other experiments, there are limited or no environmental data. In those cases, educated guesses are provided, using wordings as "possible cause," "may be due to," etc. There are also observations which are presented as is, without any explanation at all. The emphasis of this paper is on the diversity of channels, not on their causes.

A. Benign Channel

Not all acoustic communication channels are challenging. Fig. 2 gives the spreading function of an easy channel. There is only one appreciable path, or two or more unresolved paths, and no discernible Doppler spread. To confirm that this spreading function reflects a simple communication channel, a communication signal is demodulated that was transmitted shortly after the probe. The modulation is quadrature phase-shift keying, using a single carrier at 14 kHz and a symbol rate of 3500 symbols per second, which corresponds to a raw data rate of 7 kb/s. The receiver consists of detection and synchronization, basebanding, bandpass filtering, sampling at the symbol interval, and use of known training symbols to remove a phase offset and amplitude bias. The received symbols are plotted in Fig. 3. Error-free signaling is achieved at an output SNR of 11.4 dB, without any form of channel equalization.

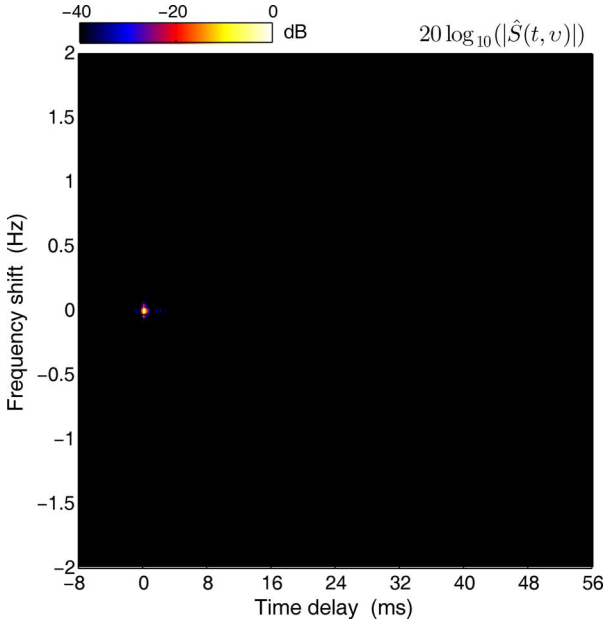

Fig. 2. Delay-Doppler spread function of a benign acoustic channel.

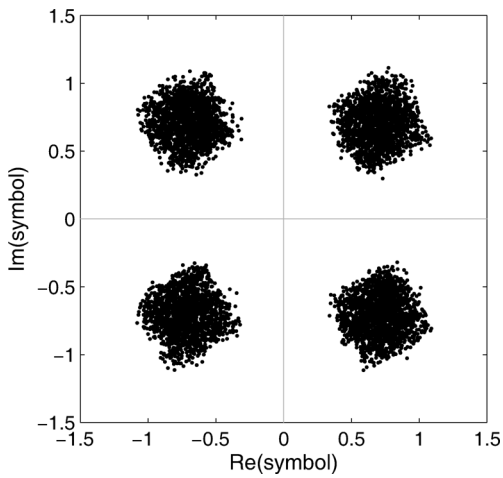

Fig. 3. Symbols at 7 kb/s, received on a single hydrophone by a textbook receiver for additive-noise channels.

B. Overspread Channel

A channel is overspread when its product of delay spread and Doppler spread exceeds one, posing a formidable challenge to phase-coherent demodulation. In the context of channel measurements, it is a channel that cannot be probed without significant measurement errors. However, if the channel is stationary, it is possible to estimate, with reasonable fidelity, Doppler spectrum and delay profile separately with different probes. This was done for the channel in Fig. 4. A $T = 16$ ms PN probe is used for the spectrum, and a $T = 128$ ms LFM probe is used for the delay profile. Whether a channel is considered to be overspread depends on the definitions of delay spread and Doppler spread. The channel in Fig. 4 is overspread using -10 dB and 90% energy definitions [15].

The dots in the top-left panel are the measured wideband spectrum, and the solid line is a compressed-exponential curve fit [15] with $P(\upsilon) \propto \exp(-|\upsilon/\alpha|^{\beta})$. The fitting parameters are $\alpha = 8.6$ Hz and $\beta = 1.6$, which is the closest to a Gaussian distribution of all spectra measured in the seven-year survey. The large Doppler spread results from an upward-refracting sound-speed profile due to cooling of the water column by the onset of Scandinavian winter. Most of the signal energy is received via surface reflections, at a significant waveheight of 1 m, and there are no noteworthy stable arrivals.

The delay profile has some aliasing and is affected by channel fluctuations within a sounding pulse, but nonetheless it gives a reasonable idea of the actual profile.

The figure also contains estimates of the temporal coherence. The round markers represent the channel autocorrelation function (5) using $\hat{h}(t,\tau)$ obtained with the PN probe, and the square markers represent the instantaneous correlation function (6) relative to an instant t_0 halfway the PN probe. As a third opinion, the autocorrelation function of a 32-s sine wave, transmitted shortly after the PN probe, is also included. This tonal has a frequency of 14 kHz, corresponding to the center frequency of the wideband probe. The good match between the narrowband and wideband autocorrelation functions lends credibility to the wideband sounding, and the similarity of all three estimates is in agreement with a stationary channel. The channel coherence time may be defined as the time it takes for the correlation to drop from 1 to 0.5, and is as short as 30 ms.

At 80 b/s and high SNR, spread-spectrum communication signals with channel coding could not be decoded correctly with a chip-rate decision-feedback equalizer (DFE) [77], not even with the equalizer in training mode. The contrast with the underspread channel of the previous section is tremendous. The type of channel illustrated by Fig. 4 is unfortunately not rare, at least not in Norwegian waters, and was encountered during four sea trials in three areas.

C. Specular Paths

In terrestrial wireless communications, a line-of-sight path is often called a specular path. A key property of such a path is that its amplitude and phase are constant on the time scale relevant to the communication system. In underwater acoustic channels, specular arrivals may occur in the form of refracted paths, bottom reflections, and reflections from other static objects such as quays, rocks, and ice covers. Such paths are not necessarily static, because of possible sound-speed fluctuations in the water column, but they were often very stable during the present survey. Fig. 2 presents a channel with only specular energy, and Fig. 4 shows a channel with negligible specular energy.

A more common condition in shallow-water waveguides is a mixture of specular paths and surface reflections. The Doppler spectrum in Fig. 5 has a sharp peak at 0 Hz that reflects the static part of the channel, sidelobes at ± 0.6 Hz corresponding to the dominant frequency of the surface gravity waves [51], and a continuum of weaker sidelobes. The correlation functions fall off rapidly from a value of 1 to 0.6, and then remain practically constant. Since autocorrelation scales with energy, this tells that the specular paths carry 60% of the total signal power. The time-varying part of the channel causes the decay from 1 to 0.6, and the static part of the channel is responsible for the residue.[3] The autocorrelation function features a weak, decaying oscillation with a period of 1.6 s, the same as the wave period. The

[3]Noise can also cause a fast initial decay [13], but in the present case, it is a property of the time-varying impulse response.

TABLE I
SUMMARY OF EXPERIMENTAL CONDITIONS

Fig.	Frequency band (kHz)	Pulse type	N	T' (ms)	T (ms)	SNR (dB)	Range (km)	Depth (m)	Environment	Month	Platform motion	Doppler correction
2	10–18	LFM	256	128	128	52	0.5	10	Bay	OCT	No	CFO
4 (spectrum)	10–18	PN	1024	16	16	15	1.2	20	Fjord	OCT	No	CFO
4 (profile)	10–18	LFM	256	128	128	15	1.2	20	Fjord	OCT	No	CFO
5,11	10–18	PN	1024	32	32	29	0.8	10	Channel	MAY	No	CFO
6	4–8	LFM	17	256	2048	34	1.6	65	Fjord	NOV	Yes	PV
7	10–18	PN	1024	32	32	27	0.9	15	Fjord	OCT	No	CFO
9,10,12,25	10–18	PN	1024	32	32	35	0.8	10	Channel	MAY	No	CFO
13,14	10–18	PN	1024	32	32	13	2.0	80	Shelf	JUN	No	CFO
15	24–32	PN	256	128	128	24	2.1	80	Shelf	JUN	Possibly	CFO
16	10–18	PN	1024	32	32	26	0.9	15	Fjord	OCT	No	CFO
17	10–18	PN	1024	32	32	28	1.0	75	Shelf	JUN	No	CFO
18	10–18	PN	1024	32	32	35	0.9	15	Fjord	OCT	No	CFO
19,20,21	10–18	PN	1024	32	32	14	1.2	10	Fjord	OCT	No	CFO
22	3–7	PN	248	128	128	11	21	250	Shelf	SEP	Yes	COG
23	2–5	PN	203	145	145	23	1.2	400	Fjord	SEP	Yes	PV
24 (RX1)	24–32	PN	1024	32	32	24	2.1	80	Shelf	JUN	Yes	CFO
24 (RX2)	24–32	PN	1024	32	32	36	0.9	80	Shelf	JUN	Yes	CFO
26 (inbound)	4–8	PN	1024	32	32	40	0.9	65	Fjord	NOV	Yes	PV
26 (outbound)	4–8	PN	1024	32	32	36	1.1	65	Fjord	NOV	Yes	PV
27	2–5	PN	23	1170	1170	13	51	70	Baltic	SEP	Yes	COG
28	2–5	PN	23	1170	1170	1	16	70	Baltic	SEP	Yes	COG
29	4–8	LFM	17	256	2048	24	3.9	75	Fjord	NOV	No	CFO
30	4–8	PN	1024	32	32	24	2.0	65	Fjord	NOV	No	CFO
30	12–20	PN	1024	32	32	20	2.0	65	Fjord	NOV	No	CFO
30	24–32	PN	1024	32	32	16	2.0	65	Fjord	NOV	No	CFO

instantaneous correlation and the autocorrelation are in good agreement, which suggests that the channel is stationary over the sounding duration. A more rigorous assessment of channel stationarity can be performed by comparing all quantities defined in Section II-A between the first and second halves of the received probe signal. The channel passes as stationary, over the 32-s signal duration (not shown).

Transmission of a communication signal through this channel results in a mean square error (MSE) of about -14 dB at the output of a chip-rate DFE. If the equalizer coefficients are frozen, here arbitrarily at 1.6 s in the signal, the MSE rapidly increases and becomes weakly modulated by the wave period. The specular paths are responsible for the fact that the MSE subsequently remains stable at ≈ -11 dB.

D. Reverberation

The power delay profile in Fig. 6 features a number of sparsely distributed initial arrivals, followed by a dense reverberation tail. Such tails are due to diffuse scattering with possible contributions from a rough seafloor, a rough sea surface, and inhomogeneities within the water column. Extended reverberation tails pose challenges to channel modeling, channel measurements, and acoustic modems. The discrete arrivals are often reproduced well by 2-D propagation models for the vertical plane, but modeling of (local or global) tails may require a 3-D model to account for the possibility of out-of-plane scattering [45], [78]–[80]. Reverberation tails can be evident from the time series [81] or spectrogram of a received signal, but in channel measurements they are missed when the tracking period of the probe signal is shorter than the tail. The tail is then aliased and ends up as clutter in between, and on top of, the dominant arrivals.

In the profile of Fig. 6, it takes 32 ms to collect 60%, and 128 ms to collect 80% of the total signal power. For a communications receiver, it is particularly challenging to harvest the energy from a diffuse tail. Long equalizers are required, and the problem is aggravated in waveguides with multiple surface interactions, as Doppler spread may then increase, and coherence may decrease with delay [16], [17], [26], [52]. Some incoherently scattered paths may still be useful for coherent communications [82], but there will be remaining signal energy that acts as noise with practical communication systems.

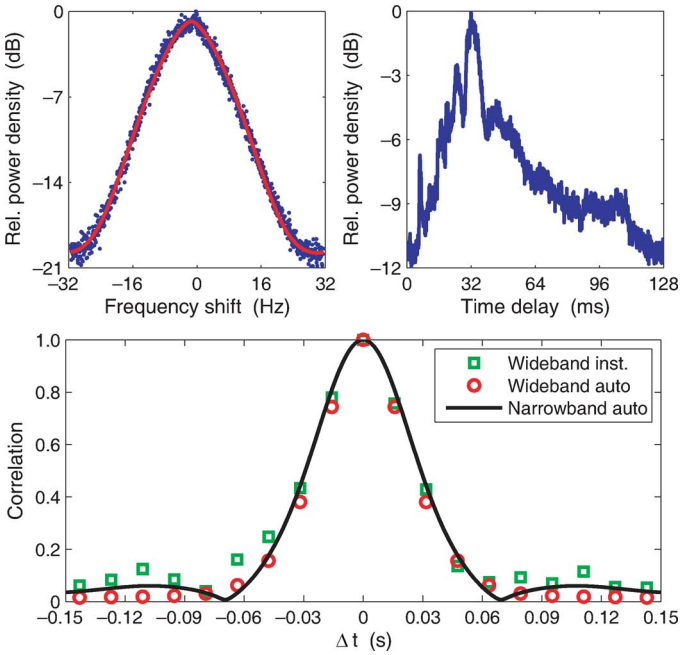

Fig. 4. Doppler spectrum, power delay profile, and normalized correlation function estimates of an overspread channel.

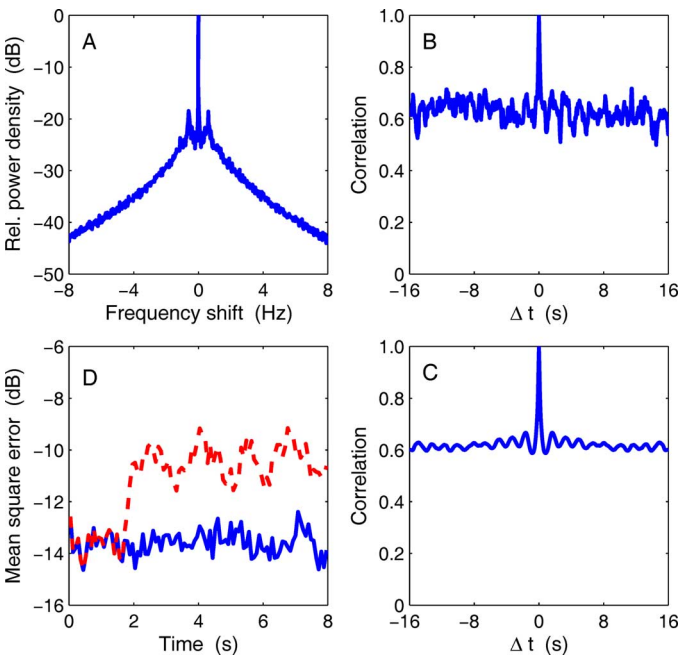

Fig. 5. A channel with a mixture of specular and fading paths. (a) Doppler spectrum. (b) Instantaneous correlation function. (c) Autocorrelation function. (d) Receiver performance with continuous tracking (solid curve) and frozen equalizer coefficients (dashed curve). The MSE is shown after despreading (seven-chip code, 1 kb/s, single hydrophone).

E. Nonstationary Channel

Fig. 7 shows a channel with a specular path, followed by clusters of arrivals having experienced one or more surface reflections. The cluster at $\tau = 12$–16 ms ceases to exist at $t = 24$ s, and soon after the cluster at 3–7 ms becomes weaker. The vanishing of signal energy coincides with the onset of the wind burst shown in Fig. 8. The suspect loss mechanism is the formation of a subsurface bubble screen due to breaking waves, which screens the ocean surface [62]. A squall of similar strength was

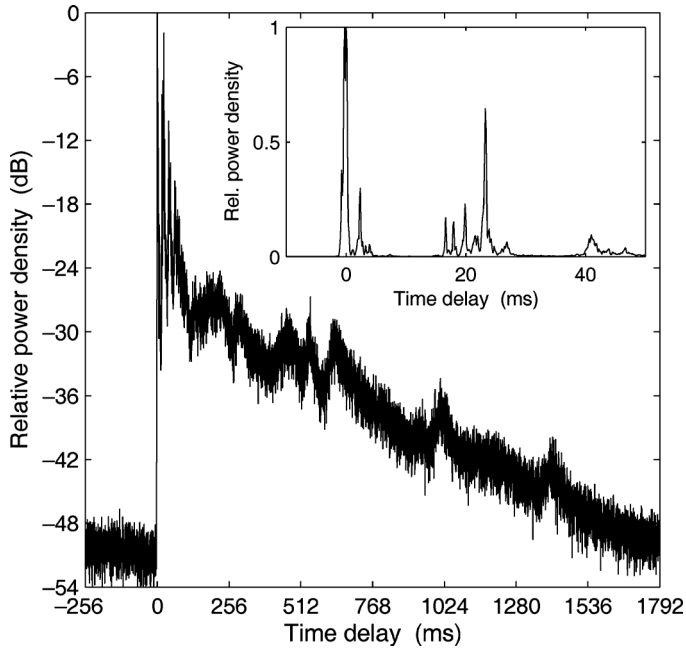

Fig. 6. Delay profile with discrete initial arrivals and a dense reverberation tail. The main graph uses a logarithmic power scale; the inset zooms in on the main arrivals and uses a linear power scale.

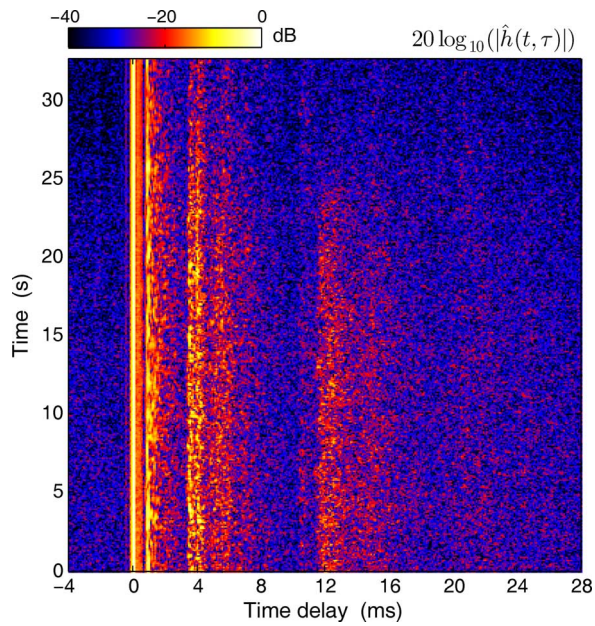

Fig. 7. Nonstationary channel. In absolute time, the attenuation at 12–16 ms sets in at 21:39:30Z (cf., Fig. 8).

shown to populate the top few meters of Loch Ness with air bubbles within a time span of 2 min [58]. Simulations [46] suggest that bubble extinction, which is the combined effect of absorption and scattering by air bubbles, may be the dominant effect in the channel of Fig. 7. Other causes of signal attenuation associated with squalls are surface waves, and bubbles due to concurring precipitation [50].

When the bubble screen of a breaking wave penetrates the entire water column, complete outage may occur [2], [61]. This was also observed with the wakes of container ships, which repeatedly terminated an acoustic communication link traversed by a shipping lane [32]. Indeed, dense bubble clouds seem to

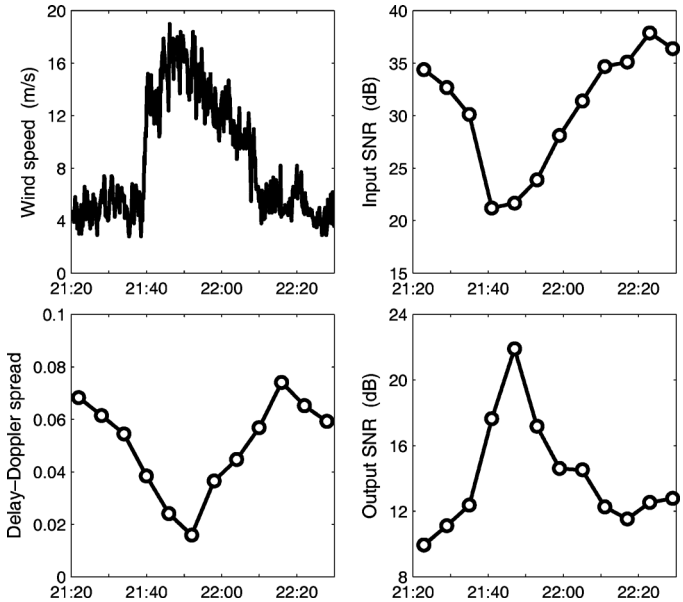

Fig. 8. Effect of a wind burst on a communication system. The delay-Doppler spread is here defined as the product of the RMS delay spread and the RMS Doppler spread. The modulation scheme is the same as in Section IV-C, and the output SNR of the single-hydrophone receiver is given after despreading.

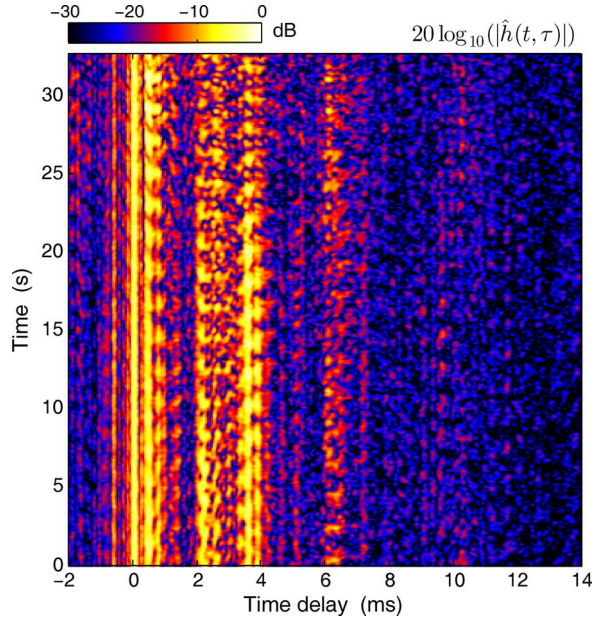

Fig. 9. Channel with cyclostationary features and correlated scattering.

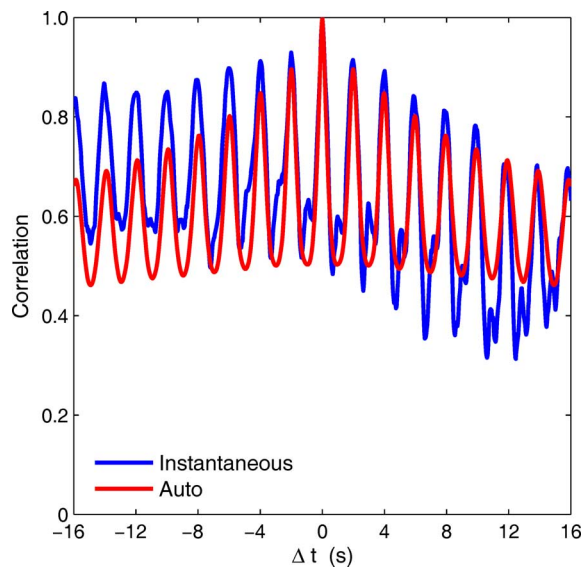

Fig. 10. Correlation function of the channel depicted in Fig. 9.

be a common feature of all ship wakes [83]. In the present case, there is no complete outage, because the specular path at $\tau = 0$ ms in Fig. 7 survives. Fig. 8 shows that the quality of a communication link actually improves significantly during the wind burst, in spite of a 15-dB reduction in SNR at the input of the receiver. The reason is a sizable drop in delay-Doppler spread, which outweighs the drop in SNR.

It is well known that the input SNR alone does not permit reliable performance prediction of acoustic communication systems, which are typically limited by reverberation [1]. Sometimes, the receiver output SNR remains well below the input SNR even with array processing [32], [33], [81], [84]. The inverse relationship between input and output SNR in Fig. 8 particularly emphasizes the need to take into account the delay and Doppler spreading in channel models and simulations. Siderius *et al.* achieved impressive agreement between measured and modeled error rates, by taking actual propagation conditions into account [18].

F. Cyclostationary Channel

The channel in Fig. 9 has repeating structures in time. A possible cause is the wake of a passing ship, which can be heard in the recording. Ship-generated waves have different characteristics from wind-generated waves, and may be characterized by distinct peaks in the spectrum [85], sometimes with higher harmonics [86]. A narrow wave spectrum corresponds to waves with a long coherence length and a sharply defined wave period. Channel fluctuations due to surface interactions may then inherit the strict periodicity of the waves.

The cyclostationary character is confirmed by the channel correlation functions in Fig. 10. Both curves are oscillating, with an envelope that falls off away from the maximum. However, in contrast to the correlation functions shown in Figs. 4 and 5, the instantaneous and averaged correlation functions are clearly different. This points to an overall nonstationary channel. This is also visible with the naked eye in Fig. 9, as the first and second halves of the sounding yield noticeably different channels. The time scale of the changes is in agreement with the hypothesis of a ship wake, which is a transient phenomenon.

G. Correlated Scattering

In the following, correlated scattering is understood to mean correlation between amplitude and phase fluctuations of physical paths. A channel with uncorrelated scattering is shown in Fig. 11 via the cross-correlation matrix defined by (8). The only significant correlation is the autocorrelation along the diagonal. On the other hand, the channel of Fig. 12 is said to have correlated scattering. Significant correlation occurs for many combinations of paths. These two channels were measured for the same signaling track, and have similar arrival structures. Fig. 11 is the cross-tap correlation for the channel of Fig. 5 and Fig. 12

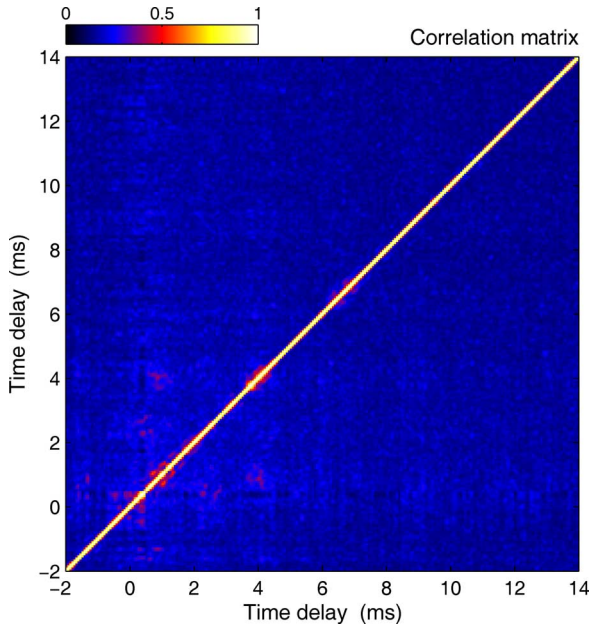

Fig. 11. Channel with uncorrelated scattering.

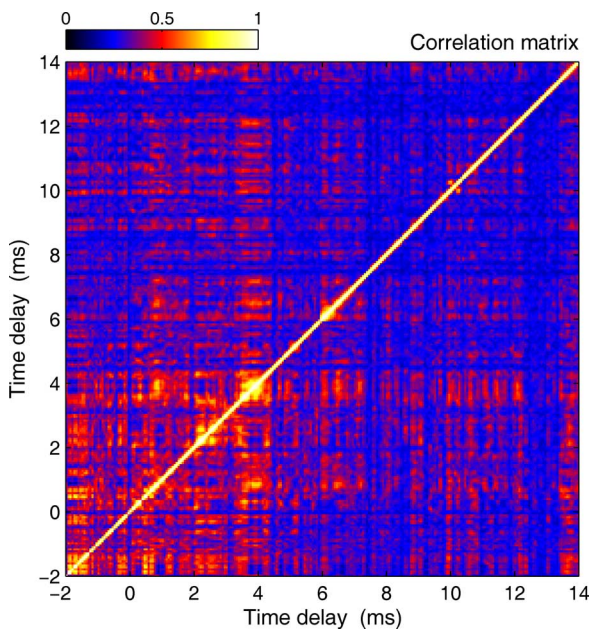

Fig. 12. Channel with correlated scattering.

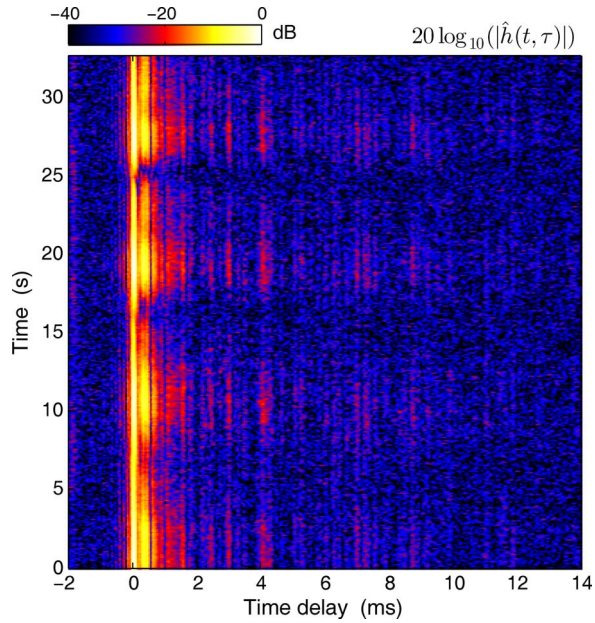

Fig. 13. In-phase, cyclostationary correlated scattering.

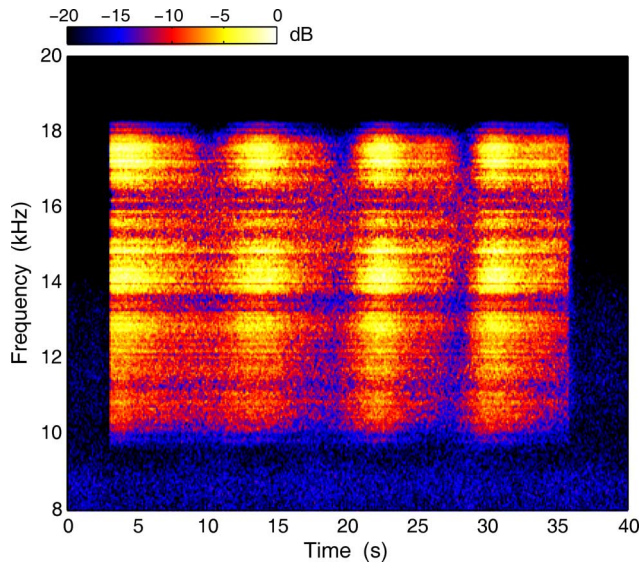

Fig. 14. Frequency-flat fading illustrated by a spectrogram of the probe signal used for Fig. 13.

for the channel of Fig. 9. The presumable cause of the correlation is the same as that of the cyclostationarity: a long coherence length of surface waves, so that paths reflected by different parts of the sea surface are correlated.

H. Frequency-Flat Fading

Another case of cyclostationary correlated scattering is seen in Fig. 13, which is a channel probed on the Norwegian continental shelf. The cycle period of 9 s agrees with the wave period measured by a waverider buoy. An important difference with Fig. 9 is that the amplitude fluctuations of the arrivals are in phase. The result is a flat fading channel, in which all frequencies of a wideband signal fade simultaneously (Fig. 14). The waves modulate the signal level and yield a time-varying SNR, similar to the signal amplitude fluctuations due to ocean swell observed by Weston *et al.* [30]. A network link may be characterized by a "hit-and-miss" connectivity. Surface waves may also result in a wave-periodic link quality via channel dynamics instead of SNR [2], [74].

I. Frequency-Selective Fading

The spectrogram in Fig. 15 is due to the interplay between two closely spaced multipath arrivals: a specular path and a surface-reflected path. Similarly to Fig. 14, it bears a strong signature of the wave period. The manifestation of the waves is different, however, as the fades in the signal spectrum are now dependent on time and on frequency. This example channel is chosen for clarity of the effect. When there are multiple paths and larger

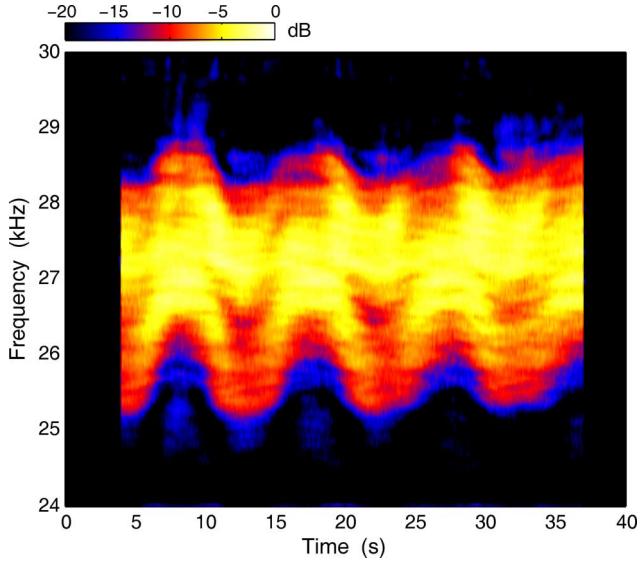

Fig. 15. Illustration of frequency-selective fading.

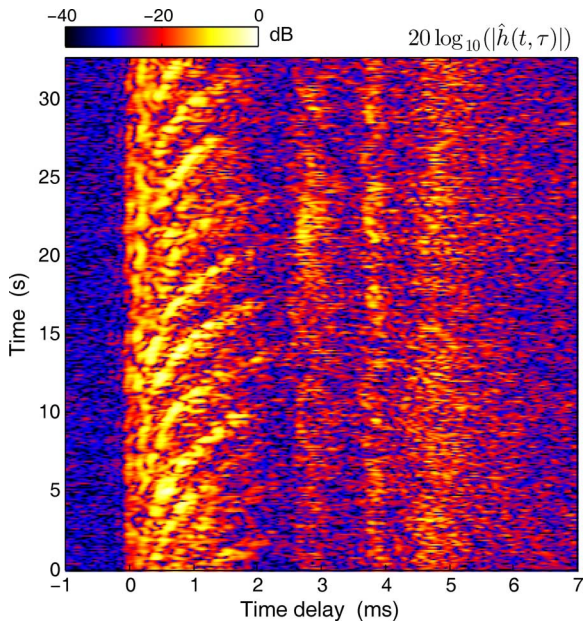

Fig. 16. A channel featuring paths with an increasing delay.

travel-time differences, there may be many fades over the band of a wideband signal.

J. Time-Varying Delays in a Stationary Deployment

The channels in Figs. 16 and 17 are characterized by arrivals with an increasing delay. Fig. 16 is a fjord measurement and Fig. 17 is a channel on the continental shelf. The features are periodic with repetition times of 3 and 8 s, respectively, which agree with the dominant frequencies of wave spectra measured during these soundings. In both cases, the signaling is between fixed bottom tripods. In Fig. 17, the arrival is not a single path, but a cluster of fluctuating micropaths. The acoustic path lengths vary by approximately 3 and 12 m in Figs. 16 and 17, considerably exceeding the corresponding significant waveheights of 1.0 and 1.4 m, respectively.

It is well known that surface gravity waves cause time-varying path lengths, but these come in different varieties. Surface reflections may move back and forth in delay [41], [44], [55], occur as a pair of micropaths with range rates of opposite signs [41], or make repetitive one-way trips in delay, as in Figs. 16 and 17. Recent measurements near Kauai yield observations similar to Fig. 16, and have been qualitatively accounted for by a 2-D parabolic equation model [54]. The varying delays in [54] are explained by moving surface wave crests, which generate focused returns with a variable travel time.

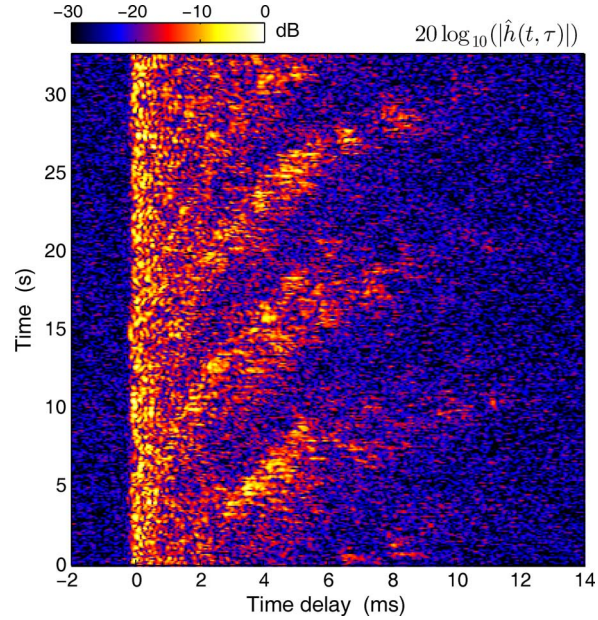

Fig. 17. A channel characterized by arrival clusters with an increasing delay.

K. Phase Drift in a Stationary Deployment

The spreading function in Fig. 18 depicts a channel with frequency offsets. A negative shift is observed for the arrival at $\tau \approx 2$ ms, where the cause is an increasing time delay, similar to Fig. 16. Simultaneously, there is an arrival with a positive shift at $\tau = 8$ ms. The paths sweep only in one direction and then cease to exist, so there is no return trip with an opposing Doppler shift. The result is a net frequency offset of these clusters in the spreading function, and the taps corresponding to these paths have a net phase drift. Note that the non-Doppler-spread specular arrival at $\tau = 0$ ms rules out CFO.

The spreading function in Fig. 19 is a dense cloud with a net frequency offset for nearly all arrivals. Visual inspection of the corresponding channel estimate in Fig. 20 does not reveal time-varying delays, but they may be obscured by the high density of arrivals or exist on a microscopic scale. Regardless of the cause, the frequency shift goes hand in hand with a significant phase drift. This is illustrated by Fig. 21, which displays the phase measurement $\hat{\theta}(t,\tau_k)$ of the channel in Fig. 20. There are many curves, because the phase is computed for all local maxima in the dense delay profile. A specular arrival at the start of the impulse response yields the curve with a constant phase. All other taps are characterized by a continuous phase drift.

An adaptive equalizer benefits from an embedded phase-locked loop (PLL) [87] in this channel. The PLL phase estimate is included in the figure for an 8-s communi-

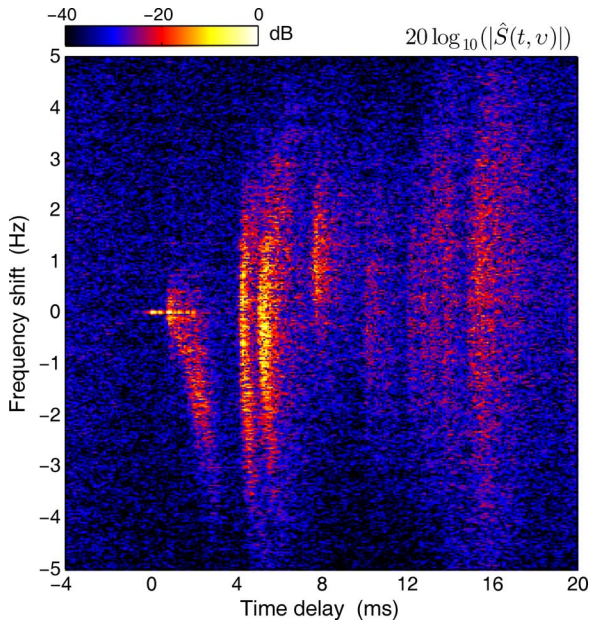

Fig. 18. Arrivals with different Doppler spreads and shifts.

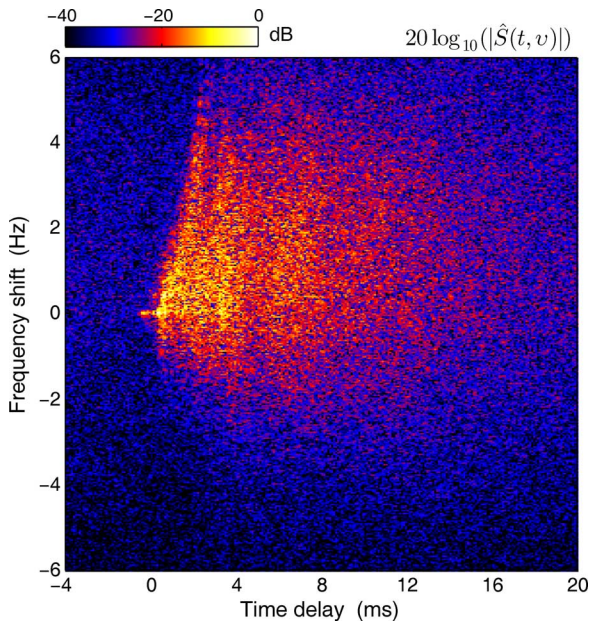

Fig. 19. A continuum of paths with a common frequency offset.

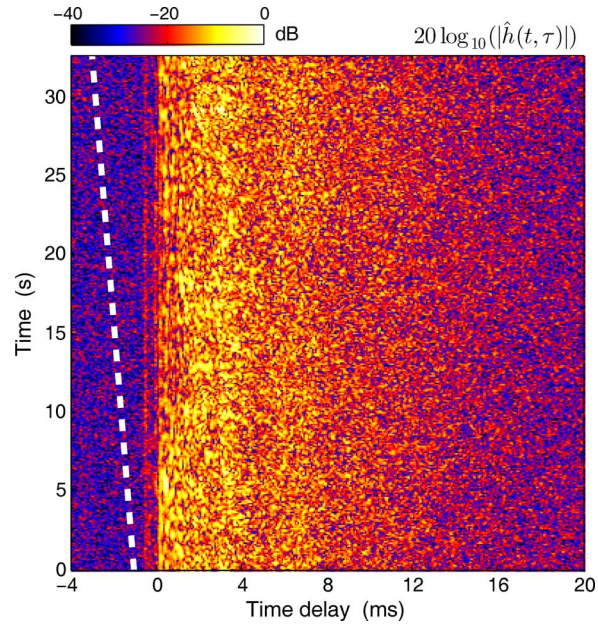

Fig. 20. The channel corresponding to Figs. 19 and 21. The dashed white line is a hypothetical path with a range rate of −0.085 m/s, which has the same phase drift as the measured channel.

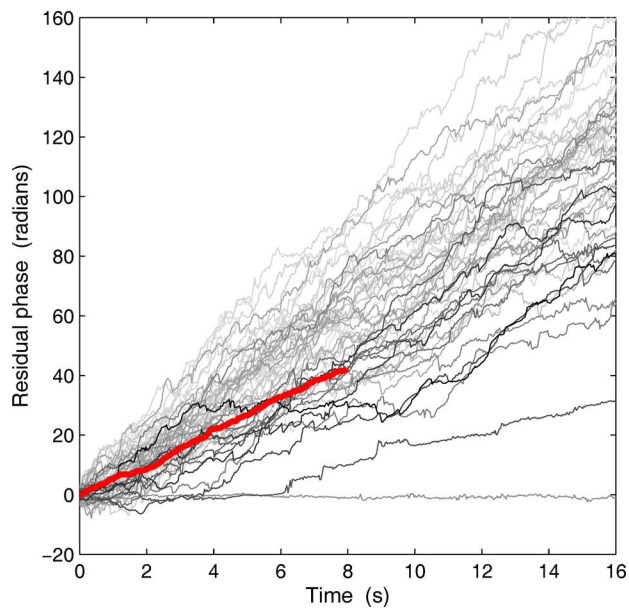

Fig. 21. Phase drift in the channel of Figs. 19 and 20. The gray shade scales with the power density in the delay profile: the more energetic the tap, the darker the curve. The thick red curve is the PLL phase estimate of a communications receiver.

cation signal transmitted after the probe, and shows that the phase drift is not a sounding artifact, but a valid measurement of relevance to the communication system. The PLL senses a phase drift of 5 rad/s.

Linear phase drifts are often due to uncompensated Doppler shifts or CFOs, which yield time compression/dilation of the signal. In that case, a phase drift $\mathrm{d}\varphi/\mathrm{d}t$ of 5 rad/s yields a Doppler shift $\Delta f = (\mathrm{d}\varphi/\mathrm{d}t)/(2\pi) = 0.8$ Hz. At the center frequency $f_c = 14$ kHz of the probe signal, this corresponds to a range rate $v = -(\Delta f/f_c)c = -0.085$ m/s, where the negative sign indicates time compression. A hypothetical path with this range rate is included in Fig. 20 as the dashed line. If overall time compression were the cause of the phase drift in the measured channel, this would be noticed. The receiver does not receive more bits per unit of time than sent by the transmitter. Resampling a communication signal is a proper receiver measure in the hypothetical channel, but not in the measured channel, although it may remove the (nominal) phase drift in both cases.

The effect was measured for downwind transmission during a period with strong winds (8–20 m/s), and lasted for more than a day. It is interesting to note that measurements of sea-surface backscatter have yielded a negative Doppler shift when transmitting downwind, and a positive shift when transmitting upwind [51]. The present forward-scatter measurement gives a positive shift for downwind transmission. A positive shift for forward-scattered surface returns is also reported in [88] (Autec

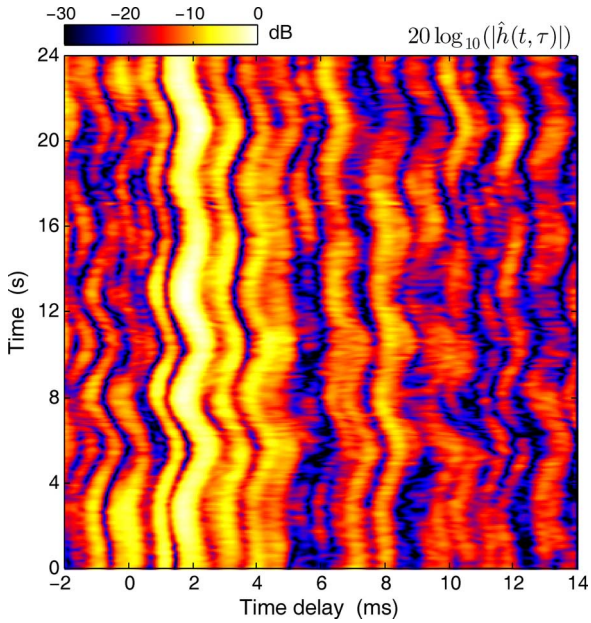

Fig. 22. Time-varying time delay due to wave-induced ship motion.

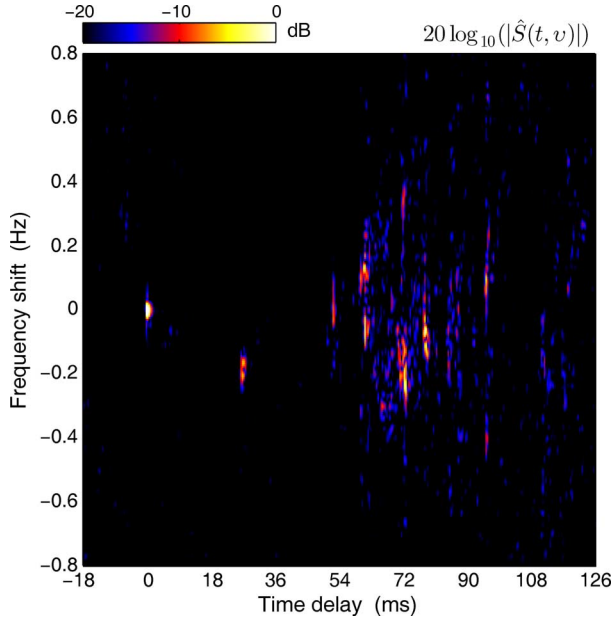

Fig. 23. Paths with constant but different range rates create a sparsely populated spreading function.

data) and [57], but these references do not mention the direction of wind and waves. The simultaneous presence of arrivals with negative and positive shifts in Fig. 18 occurred at close reach.

L. Platform Motion

So far, most propagation effects were measured between immobile senders and receivers, which implies that all Doppler effects in the data are due to variability of the medium. When either the sender and/or the transmitter is moving, this is no longer true. An example is shown in Fig. 22 for an experiment with a source towed by a surface ship. The motion of the ship on the waves is transferred onto the source, which leads to a characteristic undulating path excursion. Note that the nominal Doppler shift has been removed, so that the figure only reveals the residual time compression/dilation. The paths move back and forth, and the time-varying range rate is essentially the same for all paths. Resampling a received communication signal (with a time-varying resampling factor) would be a proper measure in this channel. Most of the Doppler spread is due to the phase variation, and a PLL alone also improves the performance of an adaptive equalizer in this channel.

As the range between the sender and the receiver decreases, the contribution of paths with steeper ray angles grows. Range rates start to differ between paths, and the received waveform becomes a sum of signal copies with different delays and different Doppler shifts. Fig. 23 exemplifies such a channel via the spreading function. This sounding also uses a towed source, but the sea surface is calm and linear motion dominates. The channel is sparse in delay and in Doppler, and a showcase for the "multiscale multilag" channel model [89], [90] and channel estimation methods exploiting sparsity in delay and/or Doppler [91], [92]. Note the contrast with the densely populated spreading function in Fig. 19. The discrete Doppler offsets imply that the arrival times are steadily changing. The delay profile changes with time in this nonstationary channel.

The motion of another type of platform is illustrated by the phase measurement in Fig. 24. In this experiment, the sender was suspended 2.5 m above the seafloor between a bottom weight and the buoyancy of a submerged float. The residual phase, shown only for the dominant path, demonstrates that this type of deployment does not qualify as a stationary setup. Unintended transmitter motion, due to current, causes a time-varying range and a corresponding undulating phase. To remove possible doubt about the origin of the effect, the phase measurement is shown for reception on two receivers, R1 and R2. Both receivers were mounted on tripods on the seafloor. R1 was deployed 2 km east, and R2 was deployed 1 km west of the transmitter. The curves look very similar, but have opposite signs, because movement away from R1 is movement toward R2, and *vice versa*. Trend removal, to mitigate uncompensated CFO, and inverting the R2 phase result in the dash–dot curves. These curves show that the phase variation is precisely the same, and that transmitter motion is the only plausible explanation.

The Doppler variance of signals received from this transmitter was strongly correlated to tidal currents during an eight-day deployment, and the contribution of transmitter motion to the total Doppler spread was much larger than that of the medium. Likewise, current-induced movement of acoustic modems was the main cause of packet errors for network links studied in Singapore waters [67].

M. Shape of the Doppler Spectrum

Part of the channel soundings in Norwegian waters yield symmetrical Doppler spectra, frequently with a characteristic stretched or compressed exponential shape [15]. The spectrum in Section IV-B is an example. Other examples of symmetrical spectra are found in Sections IV-C and IV-O. An almost symmetrical spectrum with a very different shape is shown in Fig. 25. This is the spectrum of the cyclostationary channel with correlated scattering exhibited in Fig. 9, whose correlated

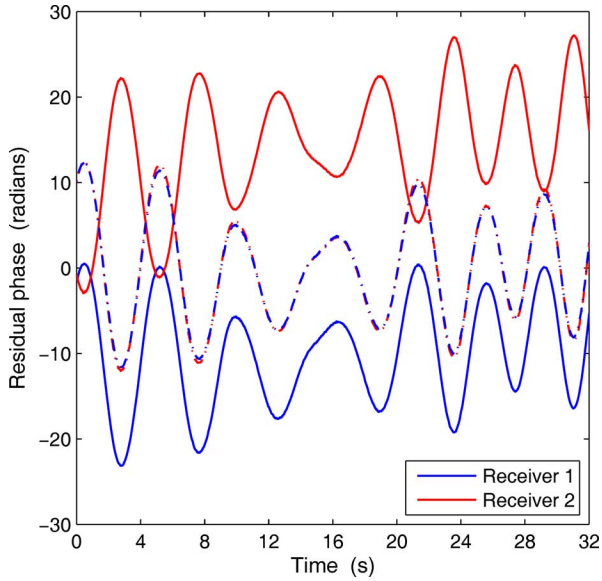

Fig. 24. Phase oscillation due to current-induced transmitter motion. The two dash–dot curves result from trend removal and inversion of the R2 phase. The time is measured from the start of the received signal, on each receiver.

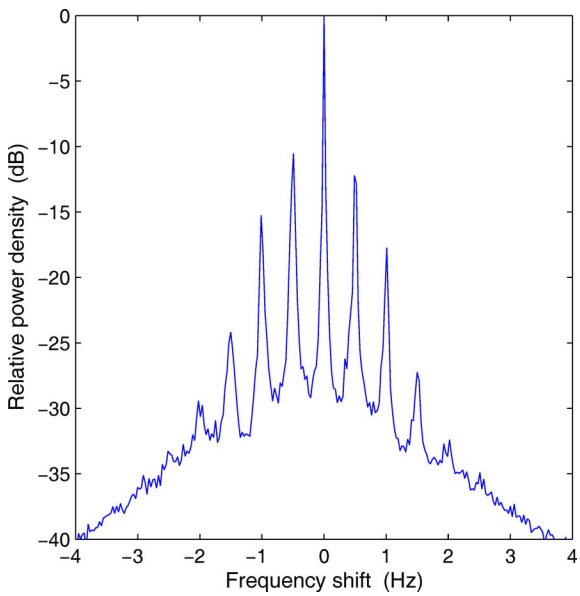

Fig. 25. Spectrum with sharp sidelobes and higher harmonics.

scattering is shown in Fig. 12. There are sharp and distinct sidelobes which may reflect a peaked surface wave spectrum, including higher harmonics possibly due to multiple surface bounces. Another possibility is the presence of multiple harmonic peaks in the wave spectrum itself [86].

On other occasions, the Doppler spectrum is markedly asymmetrical. A possible cause in stationary deployments is one-way excursions in delay due to surface waves, such as shown in Fig. 16. These correspond to true Doppler shifts that give rise to frequency offsets in the spreading function, as in Fig. 18. The offset and asymmetry observed in Fig. 19 may be due to the same cause.

Another common cause of spectral asymmetry is platform motion. The spectra in Fig. 26 are from an experiment with a towed source and a tripod bottom receiver. The sender is moving

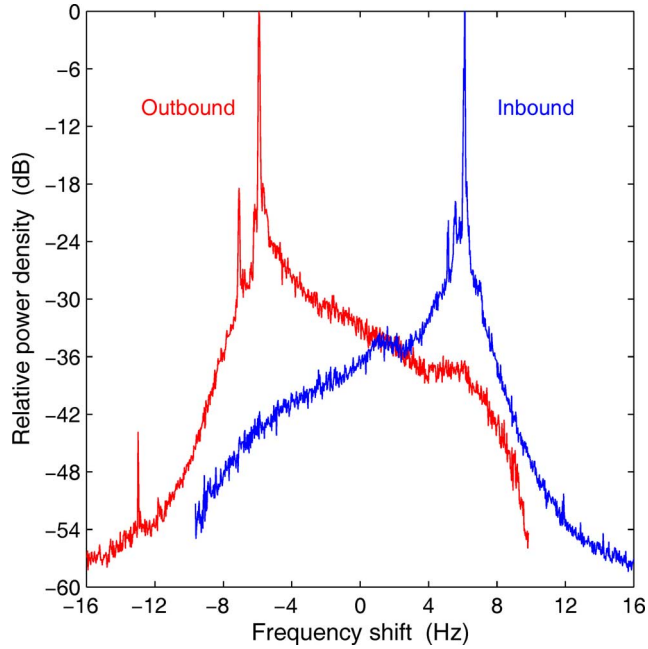

Fig. 26. Asymmetrical spectra for inbound and outbound runs with a towed source. The two spikes in the outbound spectrum are presumably interference.

toward the receiver in the inbound run, and away in the outbound run. The tow speed is $|v| \approx 1.5$ m/s in both cases, and the ranges are comparable. In this plot, the nominal Doppler shift is reinstalled after computation of the spectra, so that they peak at $-(v/c)f_c$. The inbound run yields excess power density at frequency shifts below the peak value, and the outbound run yields excess power density at frequency shifts above the peak value. This can be understood from the fact that reflected and scattered paths have larger inbound range rates, and smaller outbound range rates, than the direct path. The inbound run yields a small amount of signal energy with a negative Doppler shift, and the outbound run yields a small amount of signal energy with a positive Doppler shift. This may be due to backscatter of sound originally propagating away from the receiver.

N. Sound Channel

The measurements shown so far concerned waveguides confined by the seafloor and sea surface, or surface ducts. Part or all of the received signal energy has Doppler spread due to surface interactions, with the exception of the channel in Fig. 2. A different type of communication channel is a submerged sound channel, formed by a local minimum in the sound-speed profile. It is best known from the deep waters of the ocean, where it is known as the deep sound channel. However, sound channels may also occur in shallow waters and permit a modem signal to travel long distances, sometimes without surface or seafloor interactions. As a result, all paths may have a comparable fading rate [15]. This yields a spreading or scattering function with a separable delay profile and Doppler spectrum, $|S(v,\tau)|^2 = P(\tau)P(v)/P$, where P denotes the total signal power. Separable scattering functions simplify simulation of communication channels [26], [43].

Another characteristic of sound channels is that the shortest paths have the longest travel times, because they travel near the channel axis, where the sound speed is at a minimum. Steeper

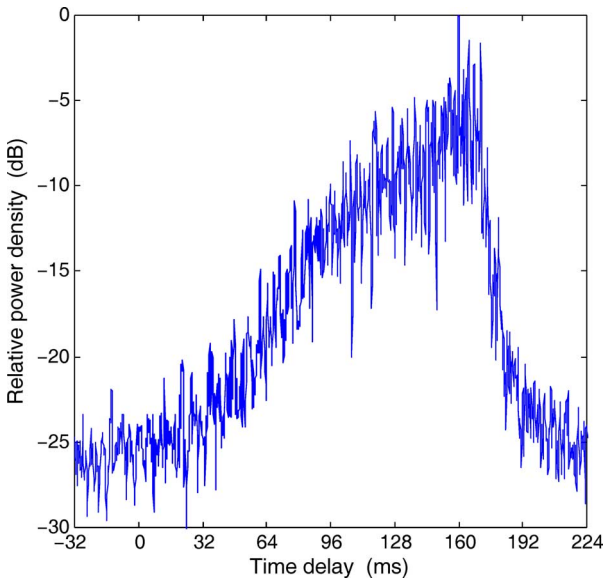

Fig. 27. Dense delay profile for signaling in a sound channel.

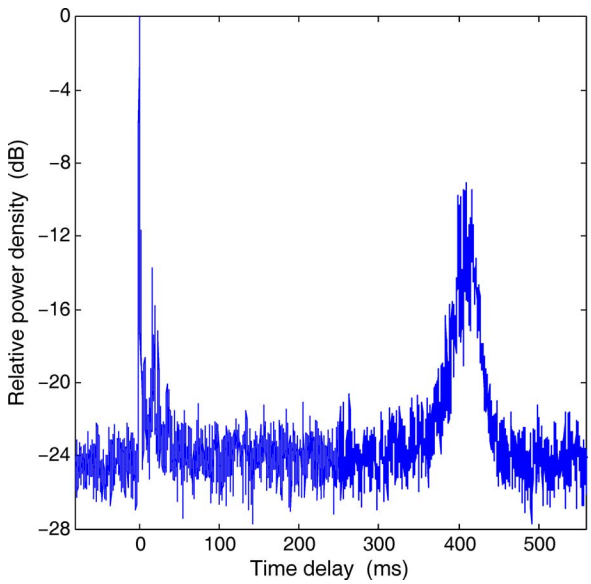

Fig. 28. Sparse delay profile measured in the Baltic Sea.

paths spend most of their travel time visiting depths at which the sound speed is greater than at the channel axis. This may result in a dense crescendo of multipath arrivals, with the most energetic paths toward the end of the delay profile. Fig. 27 gives an example from the Baltic Sea over a 51-km track with a water depth of ≈70 m. The transmitter and the receiver were placed near the channel axis at a depth of 30 m.

By contrast, a peculiarly sparse profile is shown in Fig. 28. It was registered during the same sea trial in the Baltic Sea, but with the source above the sound channel and the receiver within the sound channel. Part of the signal energy travels in a weak surface channel, whereas another part ends up in the submerged sound channel. The sound travels faster in the surface channel, but leaks into the sound channel as it propagates. As a result, both channels leave their mark on the delay profile. The precursor and the delayed cluster carry approximately the same energy, so that measures are required for high-rate communication systems. One strategy is to use sparse channel equalization [91]–[93]; another one is to use burst communication with packets shorter than the separation of 400 ms between arrivals. In the latter case, a single packet may be received twice by nodes in a network.

O. Wideband Channels

Underwater acoustic communication systems have a bandwidth that is not small compared to the center frequency of the signals and qualify as (ultra)wideband [69]. A large relative bandwidth has consequences for channel models if the propagation channel gives rise to frequency-dependent fading statistics, including the mean value of the received power. Possible causes include absorption in seawater [7]–[10], and forward scatter by the sea surface [49], [50] and seafloor [70], [71], which may cause frequency-dependent attenuation. Another cause is moving scatterers, which cause time compression/dilation of paths and frequency-dependent fluctuation rates [20]. A wideband channel is a channel that cannot be represented by the popular narrowband channel model

$$h(t,\tau) = \sum_{n=1}^{N} a_n(t)\,\delta(\tau - \tau_n) \tag{10}$$

where τ_n is the travel time of the nth path, and $a_n(t)$ is the weight with a time-varying amplitude and phase.

Since the paths in (10) have a fixed travel time, the time-varying delays in Figs. 16, 17, 22, and 23 are examples of wideband channels. In fact, most, if not all, of the preceding channels are at least somewhat wideband. This section looks explicitly at the frequency dependence. The first example is shown in Fig. 29 and reveals a frequency-dependent path loss. These delay profiles are 32-s averages obtained from a single wideband (4–8-kHz) chirp probe signal with sub-band processing to obtain profiles for the 4–5- and 7–8-kHz bands. Although the profiles represent the same channel, the arrival patterns have little in common. The required channel model has correlated taps [20], [69], but not necessarily correlation between paths as in Fig. 12, and violates WSSUS. The transfer function differs between arrivals in Fig. 29, but in other acoustic channels, the paths may have approximately the same transfer function, but (still) with a frequency dependence of the mean received power. The resulting frequency-dependent transmission loss directly affects receiver performance [94] and channel capacity [95]. Sparse channel estimation methods that represent each arrival by a single tap will not capture this propagation effect.

The second example, in Fig. 30, shows frequency-dependent Doppler spectra. In this experiment, a basket containing three transducers was placed on the seafloor. All transducers transmitted a $T = 32$ ms PN probe, but on different carriers. A tripod bottom hydrophone was used to receive the three probes. The width of the spectrum clearly increases with frequency. The spectrum in the 24–32-kHz band has a small offset and is also distorted by frequency-shift aliasing.

The type of channel is the same as the channel shown in Fig. 4 and Experiment II of [20]. Virtually all signal energy is received

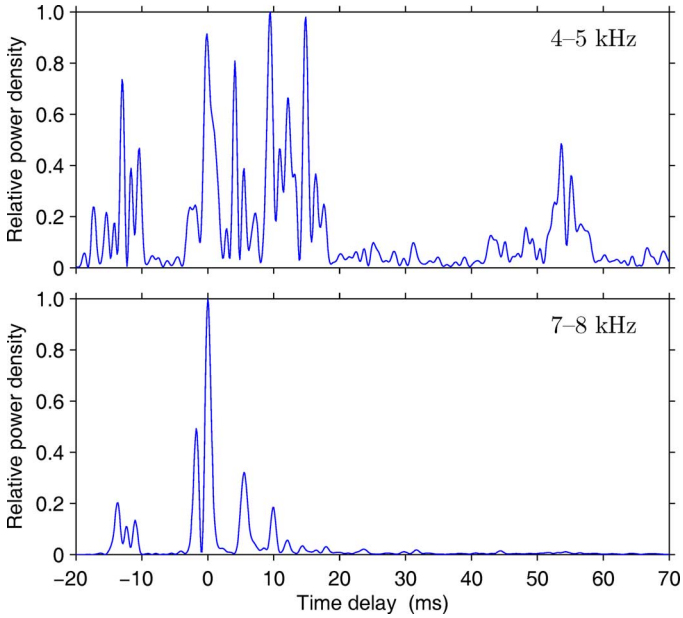

Fig. 29. Normalized delay profiles simultaneously measured in two frequency bands. The experiment and processing are described in [20].

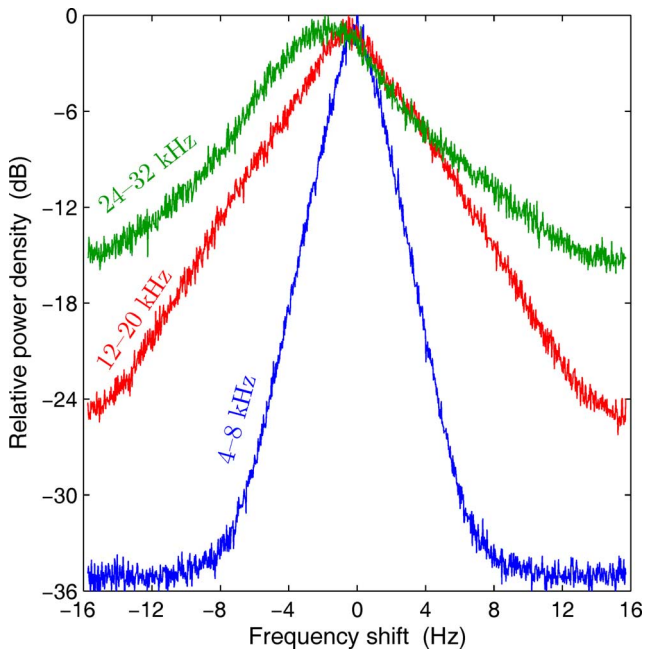

Fig. 30. Doppler spectra simultaneously measured in three frequency bands.

via reflection off surface waves, which give rise to Doppler shifts and time-varying path lengths [41], [44], [53]–[55]. A channel composed of arrivals with a distribution of Doppler scales results in a fading rate and frequency spread that increase linearly with frequency [20]. The illustration in Fig. 30 uses data from different sounders, but, of course, the Doppler spread also varies over the band of a single sounder. One should be careful with the interpretation of parameters extracted from wideband soundings. For instance, it is tempting to adopt a wideband measurement of the signal phase, or the channel coherence time, as being characteristic of the center frequency (cf., Fig. 4). If the spectrum of the received signal is skewed, however, this may not hold.

V. Summary and Conclusion

Measurements at midfrequency and high frequency (2–32 kHz) reveal a large diversity of propagation effects and scattering conditions in candidate acoustic communication channels. The importance of each effect for system design depends on both its impact on communication performance and frequency of occurrence. The impact may be different for different modulation schemes or network protocols, and how often effects occur remains to be seen, although most effects have been observed in more than one measurement campaign of the present study. One is unlikely to encounter all effects during a single mission in a given environment, but versatile acoustic modems and networks should be prepared for a wide range of conditions, specifically as follows.

- Channels range from very benign to overspread.
- The fraction of specular energy can be anywhere between 0% and 100% of the total received signal energy.
- Amplitude and phase fluctuations of the physical paths can be correlated or uncorrelated.
- Scattering can be stationary,[4] nonstationary, or have a significant cyclostationary component.
- The scattering function can be separable or nonseparable.
- Acoustic channels are inherently wideband, and may be characterized by frequency-dependent path loss, time-varying delays, and frequency-dependent fluctuation rates. Then, taps cannot be modeled independently, and the WSSUS framework is not applicable.
- Frequency-flat and frequency-selective fading may occur with wideband signals in multipath environments.
- Impulse responses can be sparse or densely populated, and include the possibility of a reverberation tail that lasts for seconds.
- The most energetic arrival may be at the start of the impulse response, at the end, or in between.
- Arrivals can stay fixed on their taps,[5] be subject to a time-varying time delay, or occur as clusters of micropaths scattered around some nominal value.
- The wideband Doppler spectrum can be symmetrical or markedly asymmetrical. It can approach a normal distribution or be sharply peaked, and may have sharp sidelobes at multiple harmonic frequency shifts.
- A coherence time as short as 30 ms at 14 kHz was measured in a stationary setting. On other occasions, the coherence time was far longer than could be measured with a 30-s probe signal.
- Continuous phase drifts and corresponding frequency shifts may occur even in stationary deployments.
- Platform motion contributes to the Doppler variance and may dwarf the Doppler spread due to the medium. The opposite can also occur.
- Platform motion yields time-varying or constant range rates, which may or may not differ between paths.
- Time-varying delays may also occur in stationary deployments, and seem to be a common feature of paths reflected off surface gravity waves.

[4]Over the typical 30-s probe signal duration. Stationarity is judged by comparison of different correlation functions, and by comparing all quantities defined in Section II-A for different segments of a probe signal.

[5]Within the measurement resolution of one over the bandwidth, and over the 30-s sounding duration.

- Surface gravity waves may modulate the level and SNR of received signals.
- Wind and waves may render a communication channel more difficult. High winds and breaking waves may render a communication channel more benign.
- Events like a wind burst, or a passing ship, may alter the scattering conditions completely on a time scale of seconds. It has also occurred that essentially the same channel was measured, for the same signaling track, in November and May.
- The SNR at the input of a receiver can be a poor indicator of the performance of the physical layer.
- Rigid mounting of transmitters and receivers is critical in order to study phase and channel fluctuations due to variability of the medium. High-frequency channel characterization with vertically suspended transducers and arrays is treacherous terrain.
- In a stationary setup, accurate resampling may be required to separate phase drifts due to possible instrument clock frequency offsets, from those due to the channel.

The reader is reminded that physical explanations of the effects were not always available, and that most of the individual statements are not new. Some may even sound trivial. The diversity of acoustic channels illustrated by the complete list, however, is still surprising.

Nothing can be taken for granted. It is often impossible to compare, in a meaningful manner, modulation schemes and network protocols from published works, as researchers perform their field tests and simulations in different settings. There is need for a set of standard test channels for the physical layer, to enable comparisons under identical, realistic, and reproducible conditions.

ACKNOWLEDGMENT

The work in this paper could not have been presented without the efforts of numerous people. The author would like to thank the consortia of the European research projects, the UUV Covert Acoustic Communications (UCAC) and the Robust Acoustic Communications in Underwater Networks (RACUN), for valuable input. T. Jenserud, R. Otnes, and M. Ainslie are acknowledged for stimulating discussions. The crews of the research vessels *Planet*, *Ocean Surveyor*, *H.U. Sverdrup II*, *HSwMS Belos*, *Nøkken*, *Småen*, *MS Strønstad*, and *M/K Simrad Echo* are acknowledged for invaluable assistance at sea. Kongsberg Maritime (Horten, Norway) is thanked for providing and programming transmitters for soundings in Norwegian waters. Comments by J. Preisig and two anonymous reviewers helped to improve the manuscript on several counts.

REFERENCES

[1] D. B. Kilfoyle and A. B. Baggeroer, "The state of the art in underwater acoustic telemetry," *IEEE J. Ocean. Eng.*, vol. 25, no. 1, pp. 4–27, Jan. 2000.

[2] J. Preisig, "Acoustic propagation considerations for underwater acoustic communications network development," *ACM SIGMOBILE Mobile Comput. Commun. Rev.*, vol. 11, no. 4, pp. 2–10, Oct. 2007.

[3] M. Stojanovic and J. C. Preisig, "Underwater acoustic communication channels: Propagation models and statistical characterization," *IEEE Commun. Mag.*, vol. 47, no. 1, pp. 84–89, Jan. 2009.

[4] G. M. Wenz, "Acoustic ambient noise in the ocean: Spectra and sources," *J. Acoust. Soc. Amer.*, vol. 34, no. 12, pp. 1936–1956, Dec. 1962.

[5] J. A. Hildebrand, "Anthropogenic and natural sources of ambient noise in the ocean," *Mar. Ecol. Progr. Ser.*, vol. 395, pp. 5–20, Dec. 2009.

[6] M. A. Ainslie, *Principles of Sonar Performance Modeling*, 1st ed. New York, NY, USA: Springer-Verlag, 2010, pp. 414–416.

[7] W. H. Thorp, "Analytic description of the low-frequency attenuation coefficient," *J. Acoust. Soc. Amer.*, vol. 42, no. 1, pp. 270–270, Jul. 1967.

[8] R. E. Francois and G. R. Garrison, "Sound absorption based on ocean measurements. Part I: Pure water and magnesium sulfate contributions," *J. Acoust. Soc. Amer.*, vol. 72, no. 3, pp. 896–907, Sep. 1982.

[9] R. E. Francois and G. R. Garrison, "Sound absorption based on ocean measurements. Part II: Boric acid contribution and equation for total absorption," *J. Acoust. Soc. Amer.*, vol. 72, no. 6, pp. 1879–1890, Dec. 1982.

[10] C. A. M. van Moll, M. A. Ainslie, and R. van Vossen, "A simple and accurate formula for the absorption of sound in seawater," *IEEE J. Ocean. Eng.*, vol. 34, no. 4, pp. 610–616, Oct. 2009.

[11] T. H. Eggen, A. B. Baggeroer, and J. C. Preisig, "Communication over Doppler spread channels—Part I: Channel and receiver presentation," *IEEE J. Ocean. Eng.*, vol. 25, no. 1, pp. 62–71, Jan. 2000.

[12] M. Badiey, Y. Mu, J. A. Simmen, and S. E. Forsythe, "Signal variability in shallow-water sound channels," *IEEE J. Ocean. Eng.*, vol. 25, no. 4, pp. 492–500, Oct. 2000.

[13] T. C. Yang, "Measurements of temporal coherence of sound transmissions through shallow water," *J. Acoust. Soc. Amer.*, vol. 120, no. 5, pp. 2595–2614, Nov. 2006.

[14] B. Tomasi, G. Zappa, K. McCoy, P. Casari, and M. Zorzi, "Experimental study of the space-time properties of acoustic channels for underwater communications," in *Proc. OCEANS Conf.*, Sydney, Australia, May 2010, DOI: 10.1109/OCEANSSYD.2010.5603667.

[15] P. van Walree, "Channel sounding for acoustic communications: Techniques and shallow-water examples," Forsvarets Forskningsinstitutt, FFI-rapport 2011/00007, 2011.

[16] T. C. Yang, "Properties of underwater acoustic communication channels in shallow water," *J. Acoust. Soc. Amer.*, vol. 131, no. 1, pp. 129–145, Jan. 2012.

[17] M. Caley and A. Duncan, "Investigation of underwater acoustic multipath Doppler and delay spreading in a shallow marine environment," *Acoust. Aust.*, vol. 41, no. 1, pp. 20–28, Apr. 2013.

[18] M. Siderius, M. B. Porter, P. Hursky, and V. McDonald, "Effects of ocean thermocline variability on noncoherent underwater acoustic communications," *J. Acoust. Soc. Amer.*, vol. 121, no. 4, pp. 1895–1908, Apr. 2007.

[19] M. Chitre, "A high-frequency warm shallow water acoustic communications channel model and measurements," *J. Acoust. Soc. Amer.*, vol. 122, no. 5, pp. 2580–2586, Nov. 2007.

[20] P. A. van Walree and R. Otnes, "Ultrawideband underwater acoustic communication channels," *IEEE J. Ocean. Eng.*, vol. 38, no. 4, Oct. 2013, DOI: 10.1109/JOE.2013.2253391.

[21] A. Radosevic, J. G. Proakis, and M. Stojanovic, "Statistical characterization and capacity of shallow water acoustic channels," in *Proc. OCEANS Conf.*, Bremen, Germany, May 2009, DOI: 10.1109/OCEANSE.2009.5278349.

[22] B. Borowski, "Characterization of a very shallow water acoustic communication channel," in *Proc. OCEANS Conf.*, Biloxi, MS, USA, Oct. 2009, pp. 1–10.

[23] W.-B. Yang and T. C. Yang, "High-frequency channel characterization for M-ary frequency-shift-keying underwater acoustic communications," *J. Acoust. Soc. Amer.*, vol. 120, no. 5, pp. 2615–2626, Nov. 2006.

[24] J. Zhang, J. Cross, and Y. R. Zheng, "Statistical channel modeling of wireless shallow water acoustic communications from experiment data," in *Proc. IEEE Military Commun. Conf.*, San Jose, CA, USA, Oct.-Nov. 2010, pp. 2412–2416.

[25] R. Nadakuditi and J. C. Preisig, "A channel subspace post-filtering approach to adaptive least-squares estimation," *IEEE Trans. Signal Process.*, vol. 52, no. 7, pp. 1901–1914, Jul. 2004.

[26] Y. Isukapalli, H. C. Song, and W. S. Hodgkiss, "Stochastic channel simulator based on local scattering function," *Exp. Lett.*, vol. 130, no. 4, pp. EL200–EL205, Oct. 2011.

[27] S. H. Huang, J. Tsao, T. C. Yang, and S.-W. Cheng, "Model-based signal subspace channel tracking for correlated underwater acoustic communication channels," *IEEE J. Ocean. Eng.*, 2013, DOI: 10.1109/JOE.2013.2251808.

[28] B. Tomasi, J. Preisig, G. B. Deane, and M. Zorzi, "A study on the wide-sense stationarity of the underwater acoustic channel for non-coherent communication systems," in *Proc. Eur. Wireless Conf.*, Vienna, Austria, Apr. 2011, pp. 1–6.

[29] F.-X. Socheleau, C. Laot, and J.-M. Passerieux, "Stochastic replay of non-WSSUS underwater acoustic communication channels recorded at sea," *IEEE Trans. Signal Process.*, vol. 59, no. 10, pp. 4838–4849, Oct. 2011.

[30] D. E. Weston, A. A. Horrigan, S. J. L. Thomas, and J. Revie, "Studies of sound transmission fluctuations in shallow coastal waters," *Philos. Trans. Roy. Soc. Lond. A*, vol. 265, pp. 567–606, 1969.

[31] D. E. Weston, K. J. Stevens, J. Revie, and M. Pengelly, "Multiple frequency studies of sound transmission fluctuations in shallow water," *J. Sound Vib.*, vol. 18, no. 4, pp. 487–497, 1971.

[32] P. A. van Walree, J. A. Neasham, and M. C. Schrijver, "Coherent acoustic communication in a tidal estuary with busy shipping traffic," *J. Acoust. Soc. Amer.*, vol. 122, no. 6, pp. 3495–3506, Dec. 2007.

[33] L. Freitag and S. Singh, "Performance of micro-modem PSK signaling under variable conditions during the 2008 RACE and SPACE experiments," in *Proc. OCEANS Conf.*, Biloxi, MS, USA, Oct. 2009, pp. 1–8.

[34] I. F. Akyildiz, D. Pompili, and T. Melodia, "Underwater acoustic sensor networks: Research challenges," *Ad Hoc Netw.*, vol. 3, pp. 257–279, 2005.

[35] J. Partan, J. Kurose, and B. N. Levine, "A survey of practical issues in underwater networks," *ACM SIGMOBILE Mobile Comput. Commun. Rev.*, vol. 11, no. 4, pp. 23–33, Oct. 2007.

[36] J. M. Jornet, M. Stojanovic, and M. Zorzi, "On joint frequency and power allocation in a cross-layer protocol for underwater acoustic networks," *IEEE J. Ocean. Eng.*, vol. 35, no. 4, pp. 936–947, Oct. 2010.

[37] D. Pompili, T. Melodia, and I. F. Akyildiz, "A CDMA-based medium access control for underwater acoustic sensor networks," *IEEE Trans. Wireless Commun.*, vol. 8, no. 4, pp. 1899–1909, Apr. 2009.

[38] F. Guerra, P. Casari, and M. Zorzi, "World ocean simulation system (WOSS): A simulation tool for underwater networks with realistic propagation modeling," in *Proc. ACM WUWNet*, Berkeley, CA, USA, Nov. 2009, DOI: 10.1145/1654130.1654134.

[39] N. Parrish, L. Tracy, S. Roy, P. Arabshahi, and W. L. J. Fox, "System design considerations for undersea networks: Link and multiple access protocols," *IEEE J. Sel. Areas Commun.*, vol. 26, no. 9, pp. 1720–1730, Dec. 2008.

[40] C. Bjerrum-Niese, L. Bjørnø , M. A. Pinto, and B. Quellec, "A simulation tool for high data-rate acoustic communication in a shallow-water, time-varying channel," *IEEE J. Ocean. Eng.*, vol. 21, no. 2, pp. 143–149, Apr. 1996.

[41] J. C. Preisig and G. B. Deane, "Surface wave focusing and acoustic communications in the surf zone," *J. Acoust. Soc. Amer.*, vol. 116, no. 4, pp. 2067–2080, Oct. 2004.

[42] M. Siderius and M. B. Porter, "Modeling broadband ocean acoustic transmissions with time-varying sea surfaces," *J. Acoust. Soc. Amer.*, vol. 124, no. 1, pp. 137–150, Jul. 2008.

[43] P. A. van Walree, T. Jenserud, and M. Smedsrud, "A discrete-time channel simulator driven by measured scattering functions," *IEEE J. Sel. Areas Commun.*, vol. 26, no. 9, pp. 1628–1637, Dec. 2008.

[44] E. A. Karjadi, M. Badiey, J. T. Kirby, and C. Bayindir, "The effects of surface gravity waves on high-frequency acoustic propagation in shallow water," *IEEE J. Ocean. Eng.*, vol. 37, no. 1, pp. 112–121, Jan. 2012.

[45] J. Senne, A. Song, M. Badiey, and K. B. Smith, "Parabolic equation modeling of high frequency acoustic transmission with an evolving sea surface," *J. Acoust. Soc. Amer.*, vol. 132, no. 3, pp. 1311–1318, Sep. 2012.

[46] H. S. Dol, M. E. G. D. Colin, M. A. Ainslie, P. A. van Walree, and J. Janmaat, "Simulation of an underwater acoustic communication channel characterized by wind-generated surface waves and bubbles," *IEEE J. Ocean. Eng.*, vol. 38, no. 4, Oct. 2013, DOI: 10.1109/JOE2013.2278931.

[47] B. S. Sharif, J. Neasham, O. R. Hinton, and A. E. Adams, "A computationally efficient Doppler compensation system for underwater acoustic communications," *IEEE J. Ocean. Eng.*, vol. 25, no. 1, pp. 52–61, Jan. 2000.

[48] A. C. Singer, J. K. Nelson, and S. S. Kozat, "Signal processing for underwater acoustic communications," *IEEE Commun. Mag.*, vol. 47, no. 1, pp. 90–96, Jan. 2009.

[49] E. Y. T. Kuo, "Sea surface scattering and propagation loss: Review, update and new predictions," *IEEE J. Ocean. Eng.*, vol. OE-13, no. 4, pp. 229–234, Oct. 1988.

[50] D. E. Weston and P. A. Ching, "Wind effects in shallow-water acoustic transmission," *J. Acoust. Soc. Amer.*, vol. 86, no. 4, pp. 1530–1545, Oct. 1989.

[51] W. I. Roderick and R. L. Deavenport, "Doppler characteristics of sea surface reflected and scattered acoustic signals induced by surface wave motion," in *Proc. OCEANS Conf.*, Victoria, BC, Canada, Oct. 1993, pp. I287–I292.

[52] P. Roux, R. L. Culver, and S. Walker, "Application of the coherent-to-incoherent intensity ratio to estimation of ocean surface roughness from high-frequency, shallow-water propagation measurements," *J. Acoust. Soc. Amer.*, vol. 127, no. 3, pp. 1258–1266, Mar. 2010.

[53] J. K. Lewis, J. Rudzinsky, S. Rajan, P. J. Stein, and A. Vandiver, "Model-oriented ocean tomography using higher frequency, bottom-mounted hydrophones," *J. Acoust. Soc. Amer.*, vol. 117, no. 6, pp. 3539–3554, Jun. 2005.

[54] M. Badiey, A. Song, and K. B. Smith, "Coherent reflection from surface gravity water waves during reciprocal acoustic transmissions," *Exp. Lett.*, vol. 132, no. 4, pp. EL290–EL295, Oct. 2012.

[55] J. Ling, X. Tan, T. Yardibi, J. Li, M. L. Nordenvaad, H. He, and K. Zhao, "On Bayesian channel estimation and FFT-based symbol detection in MIMO underwater acoustic communications," *IEEE J. Ocean. Eng.*, 2013, DOI: 10.1109/JOE.2012.2234893.

[56] L. L. Scharf and R. L. Swarts, "Acoustic scattering from a stochastic sea surface," *J. Acoust. Soc. Amer.*, vol. 55, no. 2, pp. 247–253, Feb. 1974.

[57] P.-P. J. Beaujean and G. Strutt, "Measurement of the Doppler shift in forward-scattered waves caused by moderate sea surface motion in shallow waters," *ARLO*, vol. 6, no. 4, pp. 250–256, Oct. 2005.

[58] S. A. Thorpe, "On the clouds of bubbles formed by breaking wind-waves in deep water, and their role in air-sea gas transfer," *Philos. Trans. Roy. Soc. Lond. A.*, vol. 304, pp. 155–210, Feb. 1982.

[59] M. V. Hall, "A comprehensive model of wind-generated bubbles in the ocean and predictions of the effects on sound propagation at frequencies up to 40 kHz," *J. Acoust. Soc. Amer.*, vol. 86, no. 3, pp. 1103–1117, Sep. 1989.

[60] J. C. Novarini, R. S. Keiffer, and G. V. Norton, "A model for variations in the range and depth dependence of the sound speed and attenuation induced by bubble clouds under wind-driven sea surfaces," *IEEE J. Ocean. Eng.*, vol. 23, no. 4, pp. 423–438, Oct. 1998.

[61] D. M. Farmer, G. B. Deane, and S. Vagle, "The influence of bubble clouds on acoustic propagation in the surf zone," *IEEE J. Ocean. Eng.*, vol. 26, no. 1, pp. 113–124, Jan. 2001.

[62] G. B. Deane, J. C. Preisig, and A. C. Lavery, "The suspension of large bubbles near the sea surface by turbulence and their role in absorbing forward-scattered sound," *IEEE J. Ocean. Eng.*, vol. 38, no. 4, Oct. 2013, DOI: 10.1109/JOE.2013.2257573.

[63] M. A. Ainslie, "Effect of wind-generated bubbles on fixed range acoustic attenuation in shallow water at 1–4 kHz," *J. Acoust. Soc. Amer.*, vol. 118, no. 6, pp. 3513–3523, Dec. 2005.

[64] N. M. Carbone and W. S. Hodgkiss, "Effects of tidally driven temperature fluctuations on shallow-water acoustic communications at 18 kHz," *IEEE J. Ocean. Eng.*, vol. 25, no. 1, pp. 84–94, Jan. 2000.

[65] A. Song, M. Badiey, A. E. Newhall, J. F. Lynch, H. A. DeFerrari, and B. G. Katsnelson, "Passive time reversal acoustic communications through shallow-water internal waves," *IEEE J. Ocean. Eng.*, vol. 35, no. 4, pp. 756–765, Oct. 2010.

[66] G. F. Edelmann, T. Akal, W. S. Hodgkiss, S. Kim, W. A. Kuperman, and H. C. Song, "An initial demonstration of underwater acoustic communication using time reversal," *IEEE J. Ocean. Eng.*, vol. 27, no. 3, pp. 602–609, Jul. 2002.

[67] M. Chitre, I. Topor, R. Bhatnagar, and V. Pallayil, "Variability in link performance of an underwater acoustic network," in *Proc. OCEANS Conf.*, Bergen, Norway, Jun. 2013, pp. 1–7.

[68] A. F. Molisch, "Ultrawideband propagation channels—Theory, measurement, and modeling," *IEEE Trans. Veh. Technol.*, vol. 54, no. 5, pp. 1528–1545, Sep. 2005.

[69] A. F. Molisch, "Ultra-wide-band propagation channels," *Proc. IEEE*, vol. 97, no. 2, pp. 353–371, Feb. 2009.

[70] H. DeFerrari, N. Williams, and H. Nguyen, "Focused arrivals in shallow water propagation in the Straits of Florida," *ARLO*, vol. 4, no. 3, pp. 106–111, Jul. 2003.

[71] J. W. Choi and P. H. Dahl, "Mid-to-high-frequency bottom loss in the East China Sea," *IEEE J. Ocean. Eng.*, vol. 29, no. 4, pp. 980–987, Oct. 2004.

[72] O. Diachok, "Effects of absorptivity due to fish on transmission loss in shallow water," *J. Acoust. Soc. Amer.*, vol. 105, no. 4, pp. 2107–2128, Apr. 1999.

[73] P. A. Bello, "Characterization of randomly time-variant linear channels," *IEEE Trans. Commun. Syst.*, vol. 11, no. 4, pp. 360–393, Dec. 1963.
[74] J. C. Preisig, "Performance analysis of adaptive equalization for coherent acoustic communications in the time-varying ocean environment," *J. Acoust. Soc. Amer.*, vol. 118, no. 1, pp. 263–278, Jul. 2005.
[75] R. Lutwak, "The SA.45s chip-scale atomic clock—Early production statistics," in *Proc. 43rd Annu. Precise Time Time Interval Syst. Appl. Meeting*, Long Beach, CA, USA, Nov. 2011, pp. 207–220.
[76] G. Matz, A. F. Molisch, F. Hlawatsch, M. Steinbauer, and I. Gaspard, "On the systematic measurement errors of correlative mobile radio channel sounders," *IEEE Trans. Commun.*, vol. 50, no. 5, pp. 808–821, May 2002.
[77] L. Freitag, M. Stojanovic, S. Singh, and M. Johnson, "Analysis of channel effects on direct-sequence and frequency-hopped spread-spectrum acoustic communication," *IEEE J. Ocean. Eng.*, vol. 26, no. 4, pp. 586–593, Oct. 2001.
[78] P. H. Dahl, "High-frequency forward scattering from the sea surface: The characteristic scales of time and angle spreading," *IEEE J. Ocean. Eng.*, vol. 26, no. 1, pp. 141–151, Jan. 2001.
[79] J. W. Choi, J. Na, and K.-S. Yoon, "High-frequency bistatic sea-floor scattering from sandy ripple bottom," *IEEE J. Ocean. Eng.*, vol. 28, no. 4, pp. 711–719, Oct. 2003.
[80] T. Jenserud and R. Otnes, "Reverberation tail in power delay profiles: Effects and modeling," in *Proc. OCEANS Conf.*, Bergen, Norway, Jun. 2013.
[81] J. A. Flynn, J. A. Ritcey, D. Rouseff, and W. L. J. Fox, "Multichannel equalization by decision-directed passive phase conjugation: Experimental results," *IEEE J. Ocean. Eng.*, vol. 29, no. 3, pp. 824–836, Jul. 2004.
[82] D. Rouseff, M. Badiey, and A. Song, "Effect of reflected and refracted signals on coherent underwater acoustic communication: Results from the Kauai Experiment (KauaiEx 2003)," *J. Acoust. Soc. Amer.*, vol. 126, no. 5, pp. 2359–2366, Nov. 2009.
[83] M. V. Trevorrow, S. Vagle, and D. M. Farmer, "Acoustical measurements of microbubbles within ship wakes," *J. Acoust. Soc. Amer.*, vol. 95, no. 4, pp. 1922–1930, Apr. 1994.
[84] D. B. Kilfoyle, J. C. Preisig, and A. B. Baggeroer, "Spatial modulation experiments in the underwater acoustic channel," *IEEE J. Ocean. Eng.*, vol. 30, no. 2, pp. 406–415, Apr. 2005.
[85] H. Hofmann, A. Lorke, and F. Peeters, "The relative importance of wind and ship waves in the littoral zone of a large lake," *Limnol. Oceanogr.*, vol. 53, no. 1, pp. 368–380, Jan. 2008.
[86] D. C. Wyatt and R. E. Hall, "Analysis of ship-generated surface waves using a method based upon the local Fourier transform," *J. Geophys. Res. C*, vol. 93, no. 11, pp. 14133–14164, Nov. 1988.
[87] M. Stojanovic, J. A. Catipovic, and J. G. Proakis, "Phase-coherent digital communications for underwater acoustic channels," *IEEE J. Ocean. Eng.*, vol. 19, no. 1, pp. 100–111, Jan. 1994.
[88] T. H. Eggen, "Underwater acoustic communication over Doppler spread channels," Ph.D. dissertation, Dept. Appl. Ocean Phys. Eng., Massachusetts Inst. Technol. (MIT), Cambridge, MA, USA, 1997, MIT/WHOI 97-25.
[89] S. Yerramalli and U. Mitra, "Optimal resampling of OFDM signals for multiscale-multilag underwater acoustic channels," *IEEE J. Ocean. Eng.*, vol. 36, no. 1, pp. 126–138, Jan. 2011.
[90] T. Xu, Z. Tang, G. Leus, and U. Mitra, "Multi-rate block transmission over wideband multi-scale multi-lag channels," *IEEE Trans. Signal Process.*, vol. 61, no. 4, pp. 964–979, Feb. 2013.
[91] W. Li and J. C. Preisig, "Estimation of rapidly time-varying sparse channels," *IEEE J. Ocean. Eng.*, vol. 32, no. 4, pp. 927–939, Oct. 2007.
[92] C. R. Berger, S. Zhou, J. C. Preisig, and P. Willet, "Sparse channel estimation for multicarrier underwater acoustic communication: From subspace methods to compressed sensing," *IEEE Trans. Signal Process.*, vol. 58, no. 3, pp. 1708–1721, Mar. 2010.
[93] K. Pelekanakis and M. Chitre, "New sparse adaptive algorithms based on the natural gradient and the L_0-norm," *IEEE J. Ocean. Eng.*, vol. 38, no. 2, pp. 323–332, Apr. 2013.
[94] C. R. Berger, W. Chen, S. Zhou, and J. Huang, "A simple and effective noise whitening method for underwater acoustic orthogonal frequency division multiplexing," *J. Acoust. Soc. Amer.*, vol. 127, no. 4, pp. 2358–2367, Apr. 2010.
[95] C. Polprasert, J. A. Ritcey, and M. Stojanovic, "Capacity of OFDM systems over fading underwater acoustic channels," *IEEE J. Ocean. Eng.*, vol. 36, no. 4, pp. 514–524, Oct. 2011.

Paul A. van Walree (M'08) received the M.Sc. and Ph.D. degrees in solid-state physics from Utrecht University, Utrecht, The Netherlands, in 1992 and 1997, respectively.

From 1998 to 2009, he was an Underwater Acoustician at The Netherlands Organisation for Applied Scientific Research (TNO), The Hague, The Netherlands. In 2009, he started as a Scientist with the Maritime Systems Department, Norwegian Defence Research Establishment (FFI), Horten, Norway. His research interests include digital underwater communications, channel characterization and simulation, and acoustic signal processing.